Utilizing enhanced backscattering for determination of scattering properties in turbid media
LRAP-436

David Kroon and Sara Lönn

Sammanfattning

Ljusets utbredning i material kan beskrivas med hjälp av vissa begrepp som t.ex. spridning och brytningsindex. Ljus sprids, d.v.s ändrar utbredningsriktning, då det färdas genom en yta mellan två medium i vilket det har olika utbredningshastigheter. Ljusets hastighet i ett medium anges med hjälp av brytningsindex vilket anger hur många gånger fortare ljuset färdas i vakuum.

Ett exempel på spridande material är moln, som är uppbygga av väldigt små vattendroppar. Skillnaden mellan vattnets och luftens brytningsindex leder till att ljuset kommer att ändra sin utbredningsriktning otaliga gånger i ansamlingen av de små vattendropparna. Högt spridande material upplevs ofta som vita till färgen just på grund av det stora antalet spridningar som sker i materialet. Andra exempel på spridande material är papper, mjölk och läkemedelstabletter.

För att optiskt kunna göra kemiska analyser av högt spridande material är det viktigt att känna till materialets optiska egenskaper. Sådana metoder har tillämpningar inom t.ex. det medicinska området där man optiskt vill kunna undersöka vävnad, som är mycket spridande. Ett annat tillämpningsområde är kemisk analys av läkemedel som på grund av sin porösa struktur också är spridande.

Det här projektet handlar om hur ett materials spridningsegenskaper kan mätas med hjälp av ett fysikaliskt fenomen som kallas förstärkt bakåtspridning (*enhanced backscattering*). Materialen kan betraktas som uppbyggda av ett stort antal spridare i en oordnad struktur. Vågorna kommer att spridas slumpmässigt flera gånger på sin väg genom materialet. En del av ljuset kommer att spridas bakåt, ut genom den yta vilken det infallande ljuset belyser. Då ljuset sprids rakt bakåt, vid vinkeln noll, kommer det att bli förstärkt och intensiteten kommer att dubbleras. Förstärkningen av ljuset uppkommer genom att vågor som färdas samma väg genom materialet, men i motsatt riktning, förstärker varandra. Man säger då att vågorna interfererar med varandra. Förstärkningen avtar snabbt för större vinklar, vilket skapar en skarpt konformig intensitetsprofil kring små vinklar. Bredden på intensitetskonen beror på den genomsnittliga spridningslängden, d.v.s avståndet en våg färdas mellan två spridningstillfällen.

Under projektets gång har en optisk uppställning byggts för att kunna mäta den förstärkta bakåtspridningen. Genom dessa mätningar kan den genomsnittliga spridningslängden uppskattas.

Contents

Chapter 1

Introduction

1.1 Background and motivation

The investigation of light transport in highly scattering disordered materials is of great interest in many areas of research. One of those is the pursuit of reliable methods for spectroscopic chemical analysis of turbid media. Such methods find their applications in e.g the medical field where the analysis of human tissue, which is highly scattering in the visible wavelength range, is of great interest. Another area of application is chemical analysis of solid pharmaceutical materials which, due to their porous structure, often is highly scattering.

By using traditional absorption spectroscopy it is possible to decide the concentration of the chemical constituents of a substance, given that their absorption spectra and the optical path length through the sample is known. If the scattering is negligible the attenuation of the light depends on the concentration and optical pathlength through a simple relation. However, if the sampled substance is scattering the optical path length of the light is undefined. Each detected photon has taken an individual path from the source to the detector via successive random scattering events. This results in a distribution of optical pathlengts. Of course that makes the problem more complex and calls for an understanding of light transport properties under multiple scattering.

The Biophotonics group at the Division of Atomic physics at Lund University has an ongoing project where the optical properties of highly scattering materials are investigated using a time resolved method called time-of-flight spectroscopy (TOFS) [1]. As the name indicates this technique makes it possible to determine the distribution of photon flight time for a light pulse sent trough a scattering material. The theoretical framework for describing light propagation in scattering media is diffusion. Even though this is a very simplified approximation of the underlying physical process it has proven to be both accurate and widely applicable. A combination of the theoretical statements from diffusion theory and TOFS measurements makes it possible to extract scattering and absorption properties of a material. There is, however, a slight problem with this approach. For the distribution of optical pathlengths to be extracted from a TOFS-measurement the average propagation speed of the light inside the material has to be known. Hence an good estimate of the effective refractive index is a necessity to get a valid result.

Electromagnetic radiation scatters due to spatial variations in refractive index. In a highly scattering media these variations are microscopic. In porous materials e.g. the scattering is due to the difference in light propagation speed in the solid material and the gas filled pores. A simple but intuitive model for the optical pathlength of photons traveling through a porous material is:

$$L = L_s + L_p = c_0 n_s^{-1} t_s + c_0 t_p$$

Where L is the total mean pathlength, the indices s and p stands for solid respectively pore, n_s is the refractive index of the solid material, c_0 is the speed of light in free gas and t is the mean flight time. Furthermore it is intuitive to assume that the pathlengths of the photons relates to volume fractions of solid media respectively gas as:

$$\frac{L_s}{L} = \frac{V_s}{V}$$

$$\frac{L_p}{L} = \frac{V_p}{V}$$

The accuracy of this model has been investigated in a study carried out by Svensson et al.[2]. Using the time-of-flight instrument they measured the total mean flight time of photons through a highly scattering porous sample. The mean optical pathlength through the air filled pours (L_p) was estimated using a novel technique known as GAs in Scattering Media Absorption Spectroscopy (GASMAS). It exploits the narrow absorption lines in gas as compared to solids and can therefore be detected even in diffusively scattered light. Since the strength of the absorption in the gas is known, the photon average pathlength can be extracted. This technique is described in [3].

The assumptions under investigation proved to be inaccurate. In comparison with a proven method for measuring porosity the suggested model seemed to underestimate the volume fraction of the solid material. This might be taken as an indication that the light has a tendency of preferring to propagate in the solid material. The study points out that there is a need for further effort to try to understand the microscopic nature of light propagation in highly scattering media.

One step in this direction is to investigate the optical properties of scattering media by a steady state technique, i.e time independent, in order to compare and relate the result to that from a timeresolved method such as TOFS. The main aim for this project has been to build a prototype set up for such a steady state measurement.

There are different possibilities to approach such a task. In this project we exploited a phenomena characteristic for wave propagation in disordered scattering media known as Enhanced Back Scattering (EBS). EBS manifests in a an enhancement of the intensity of diffusely back scattered waves in small angles. The phenomena is due to interference between multiply scattered waves and is also referred to in the literature as Coherent Back Scattering (CBS). The angular span over which the intensity is enhanced has been shown to be related to the scattering properties of the disordered media. Therefore, besides being an interesting demonstration of the wave nature of light, EBS can be utilized for investigation of optical properties of highly scattering media.

1.2 Scope

The main interest of the project has been to make an initial investigation of the problems and possibilities with the detection of enhanced backscattering. We have focused on constructing an optical setup for measuring angular resolved backscattering. The aim of the measurements has been to extract the scattering properties of highly scattering materials.

1.3 Outline

This report is divided into 6 chapters. Chapter 2 treats the basic theory of light propagation and explains the mechanisms of enhanced backscattering. Chapter 3 describes the optical setup, its principle components and the problems encountered during the construction. Chapter 4 describes the measurements, calibration and methods for correcting the data. It also explains how the different steps of the data analysis were carried out. Chapter 5 gives an example of a measurement series and the outcome from the data analysis. The outcome is compared to TOFS measurements. Chapter 6 discusses the performance of the system, suggests feasible improvement and justifies simplifications. Appendix A gives a short overview of the formal theory of light propagation in scattering media including the EBS theory.

Chapter 2

Theory

For the concern of this thesis there are two concepts needed to describe light-matter interaction, namely absorption and scattering. These concepts will be briefly described in the first two sections. The following sections is dedicated to light transport in turbid media and the mechanisms of EBS.

2.1 Absorption

Absorption of light is the process in which energy transported by an electromagnetic wave, is transfered to a system, e.g. an atom or molecule. The absorption of an electromagnetic quanta, a photon, brings the system from one state of internal energy to another. In atoms it is the electrons surrounding the nucleus changing their quantum mechanical wave functions that accounts for the change of state. In molecules the energy state structure is a bit more complicated. Beyond the electronic states, vibrational and rotational modes can be excited and account for a change in internal energy. The possible energy states in a quantum mechanical system are discrete, as is the electromagnetic field in a quantum mechanical description. This means that the photon energy of the field has to match the transition energy, i.e the energy difference between the initial and final state of the system, in order for the process to occur. The photon energy E is related to the wavelength λ of the radiation by:

$$E = \frac{hc}{\lambda}$$

Where h is the Planck constant and c is the speed of light in vacuum.

The reversed process, in which the system is relaxed and transferred to a lower level of internal energy by emission of a photon, is of course also possible. This will in fact always happen if the system is left undisturbed long enough. On a microscopic or single particle level the probability of an absorption event to occur is expressed by the concept of cross section. As the word implies it has the unit area and expresses the probability for an absorption event to occur normalized to an area. Absorption crossection is usually denoted σ_{abs}. On a macroscopic level it is more useful to consider how much energy that is absorbed by an ensemble of particles. This is done by introducing the absorption coefficient, usually denoted μ_a. The absorption coefficient has the unit one over

length. It describes the mean probability per unit length for a photon to be absorbed while propagating through a large ensemble of absorbing particles. The relation between the cross-section and absorption coefficient, for a homogeneous ensemble of particles, is simply:

$$\mu_a = \rho\sigma_{abs}$$

Where ρ is the density of particles.

For a material consisting of different types of absorbers the total absorption coefficient is simply the sum of the absorption coefficients for each subset, provided that the mix is homogeneous.

As the discussion above implies, the absorption coefficient is dependent on the wavelength of the interacting light and should therefore, unless it is obvious from the context, be denoted $\mu_a(\lambda)$.

As for all processes with a constant probability for an event to occur, in this case an absorption event, the attenuation of a light beam propagating through an non scattering absorbing material can be described by a exponential function.

$$I = I_0 e^{-\mu_a x}$$

This exponential relation is called the Beer-Lambert law and gives the intensity of the beam, I, after a propagation length, x, given an initial intensity I_0.

2.2 Single scattering

In this thesis we are exclusively considering elastic scattering. That is scattering processes in which the energy carried by the electromagnetic wave is preserved, or to put it differently, the scattering does not affect the wavelength of the light. For this case scattering can normally be described by classical wave theory and quantum mechanical effects do not come in to play.

An electromagnetic wave propagating through a dielectric material will continuously interact with the electrons along its propagation path. Because of this interaction the propagation speed of the wave is slowed down compared to the propagation speed in vacuum, denoted c. The ratio between the speed of light in vacuum and in the material in question is referred to as its refractive index, denoted n. On a macroscopic level, when a wave front propagates through an interface between two materials of different refractive indexes it will be refracted, i.e change its direction of propagation. This phenomena is well described in geometrical optics by the Fresnel and Snell's formulas. The validity of these formulas is, however, limited to problems where the obstacle of propagation is very large in comparison with the light wavelength. In geometrical optics one uses the notion of rays to describe light propagation. This is an approximation which is only valid if the crossection area of each ray can be allowed to be of order $l\lambda$, where l is the length over which the ray is traced [4]. For problems concerning small scale spatial variations of refractive index one has to use scattering theory.

In single scattering theory there are three important physical quantities. The most fundamental one is the amplitude function, $S(\theta, \varphi)$, which is a function of the polar angle θ and the azimuthal angle φ in relation to the propagation direction of the incoming wave. $S(\theta, \varphi)$ relates the phase and amplitude of the

scattered wave to the phase and amplitude of the incoming plane wave. The electrical field of the outgoing wave is given by the amplitude function multiplied by a normalized spherical wave and the incoming wave:

$$E_{out} = S(\theta, \varphi)\frac{e^{-ikr+ikz}}{ikr}E_0$$

Where k is the wavenumber, $k = 2\pi/\lambda$. This relation is valid for spherical symmetrical homogeneous particles and an arbitrary polarization of the light. If the scattering particle is not spherical symmetric the direction of the polarization vector in relation to the orientation of the particle of course becomes important. In that case the above expression transforms into a matrix relation:

$$\begin{pmatrix} E_l \\ E_r \end{pmatrix} = \begin{pmatrix} S_2 & S_3 \\ S_4 & S_1 \end{pmatrix} \frac{e^{-ikr+ikz}}{ikr} \begin{pmatrix} E_{l0} \\ E_{r0} \end{pmatrix}$$

When knowing the amplitude function it is easy to calculate the intensity distribution of the scattered light. The relation between the incoming light intensity and the scattered intensity distribution is given by the form factor, $F(\theta, \varphi)$:

$$I_{sca} = \frac{I_0 F(\theta, \varphi)}{k^2 r^2}$$

An integration of the form factor over all angles yields the scattering crossection of the particle, relating the total scattered intensity to the incoming intensity:

$$\sigma_{sca}(\lambda) = \frac{1}{k^2}\int F(\theta, \varphi) d\theta d\varphi$$

These three quantities do all describe the scattering event but contain declining information about the process. For a full description of the process the phase function has to be known.

The general scattering problem is difficult to solve exactly. There are, however, a few simple geometries for which it is possible to find a solution. These cases may then serve as a starting point when dealing with more complicated scattering problems.

If the scattering object's typical dimension is much smaller than the light wavelength, the electrical field over the scattering region can be viewed as homogeneous. The temporal varying field induces an oscillating dipole moment in the dielectric object, thus making it radiate at the same frequency as the incoming field. This is called Rayleigh scattering. It is characterized by its mirror symmetry in the plane of polarization as well as its strong wavelength dependent behavior. The cross section of Rayleigh scattering decreases with λ^{-4}. A common example of this type of scattering is how small particles in the earth's atmosphere scatter the blue light much more efficient than the light with longer wavelengths, hence making the sky blue in the daytime.

If the wavelength of the scattered wave is in the same range or larger than the typical dimension of the object from which it scatters, it is possible to find an exact solution to the problem, provided the object is homogeneous and the geometry is simple. Using the electromagnetic wave equation, as derived from the

Maxwell's equations, combined with boundary conditions from electromagnetic field theory the problem can be solved for spheres and cylindrical objects. This is called the Mie solution and often is characterized by forward scattering and a quite complex wavelength dependence. For example the cross-section typically peak around certain distinct wavelengths, indicating resonant scattering.

2.3 Multiple scattering

The problem of multiple scattering in a material of randomly located scatterers, has to be treated in a quite simplified way, in order to be solvable. Obviously it is not possible to account for every single amplitude function of a large set of scatterers. Secondly, randomness of the material introduces a stochastical dimension to the problem. Even if there was a way to find the intensity distribution for one configuration of scatterers this would be meaningless since it would not characterize the material as a whole. This point becomes quite clear when studying the speckle patterns of randomly scattered coherent light.

2.3.1 Speckle

A speckle pattern is a random pattern of rapidly alternating low and high intensity. This phenomena occurs when highly coherent light is scattered in a structure of random scatterers. Figure 2.1 displays an image of the angular resolved intensity distribution of highly coherent light from a HeNe laser scattered of a tablet of highly scattering TiO_2 powder in epoxy.

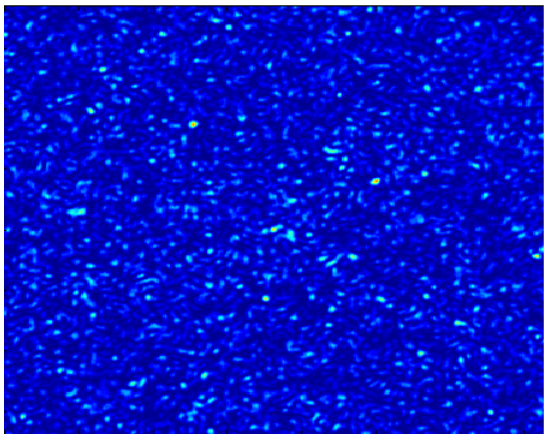

Figure 2.1: Image of a speckle pattern

Speckle occurs due to interference between waves traveling along random paths in the structure. The light intensity at one point is proportional to the absolute value of the squared sum of all the electrical fields in that point. Since all the waves contributing to the total field have traveled along separate paths, their relative phase is completely random. Adding up all the contributing waves at any point thus yields a random intensity. Let E_i be the the electrical field from a wave having traveled along a path i at an arbitrary point. The intensity in that point is proportional to the sum:

$$I \propto \left(\sum_i E_i\right)\left(\sum_j E_j^*\right) = \sum_i E_i E_i^* + \sum_i \sum_{j \neq i} E_i E_j^*$$

The first term in the resulting sum corresponds to adding up all the fields incoherently, i.e without considering the interference between them. This term can only assume positive values. The second term is the interference term, it can assume both positive and negative values. The resulting intensity distribution is a function of the location and orientation of the individual scatterers as well as the phase distribution of the incoming light. Therefore the investigation of multiple scattering has to have a statistical approach. The aim for such an approach is to find the average intensity distribution realized by averaging over several speckle patterns. When averaging the first term yields an averaged intensity distribution. The second term will average to zero, thus making most interference effects and phase relations lose their relevance [5].

To capture the average intensity distribution in an experimental situation, one has to average over several speckle patterns. If the sample material is a liquid with dispersed scatterers, the Brownian motion of the scattering particles will accomplish the averaging, provided that the integration time of the sensor is long enough to allow for substantial relocation of the particles.

If the sample material is a solid and the coherency properties of the light are not relevant for the measurement, low coherent light should be used. In a low coherent light beam the phase relation between different parts of the beam is rapidly changing to reduce the influence of speckles. This creates a time averaging on the same timescale as the phase fluctuations.

If the coherence properties of the beam are important and a highly coherent laser beam is used, the location of the scattering centers has to be continuously altered in relation to the beam to allow time-averaging of the speckles. The integration time of the sensor then has to be adjusted to match the time scale of the movement.

2.3.2 Light transport

To treat multiple scattering as stochastic process one has to introduce a material specific parameter, the scattering coefficient μ_s. The scattering coefficient expresses the probability per unit length for a photon to be scattered while traveling through the material. The inverse of the scattering coefficient is also appearing in the literature, usually denoted l, and is called the mean free path. As in the case of absorption, the scattering coefficient can be related to the scattering cross section under the condition that the scatterers see each other in the far-field, i.e. at a couple of wavelengths distance. This is necessary for the scattering events to be considered independent. The relation between the two properties can then be expressed:

$$\mu_s = \rho \sigma_{sca}$$

The scattering properties are not fully defined by the scattering coefficient. As mentioned earlier the scattered intensity has an angular dependence dictated by the size, shape and material of each independent scatterer. As we shall

see later the theory of multiple scattering is a scalar theory and can thus not account for anisotropic scattering in the plane of polarization. In the scalar case, if the scattering particle is assumed to be spherical symmetric, the only defined direction in the problem is the direction of incidence. Thus by necessity this solution is symmetric around an axis in the direction of incidence. In the vector case there are two defined directions, the direction of incidence and the polarization vector direction. This breaks the symmetry in the plane of polarization and allows anisotropic scattering. What can be accounted for, in the scalar model, is an anisotropy of the scattering polar angle θ. This is done by introducing the anisotropy factor g, the mean cosine of the scattering angle:

$$g = \langle \cos(\theta) \rangle$$

The scattering coefficient and the anisotropy factor is combined into one parameter, the reduced scattering coefficient or transport scattering coefficient μ_s':

$$\mu_s' = \mu_s(1 - g)$$

To understand the physical meaning of the reduced scattering coefficient imagine the extreme case in which $g = 1$. In this case all the light would be scattered in the propagation direction of the incoming light, thus taking away the effect of the scattering. For perfectly isotropic scattering, $g = 0$ and thus $\mu_s' = \mu_s$. $1/\mu_s'$ can also be viewed as the average distance the light has to travel in the material in order for its propagation direction to be completely randomized, called the transport mean free path.

Light transport in scattering media can, due to the particle-wave dualism of light, be view as a random photon migration process or as wave propagation in a random structure. A theoretical description of light propagation in highly scattering media can take its starting point in both views.

The most comprehensive model to work with is to consider photon migration as a random walk, neglecting the wave properties of light [1]. For most applications this description is sufficient. The other starting point of describing light propagation in highly scattering media is the scalar wave equation, corresponding to Maxwell's equations if polarization is ignored. The intensity distribution is found by a recursive expansion of the so called Dyson-Schwinger equations [5]. Both of these two approaches arrive at the same conclusion when interference effects are neglected. The result is, after some approximative assumptions, a description of light transport as a diffusion process, governed by the diffusion equation.

$$\frac{\partial \Phi(\vec{r}, t)}{\partial t} - D\nabla^2 \Phi(\vec{r}, t) + c\mu_a \Phi(\vec{r}, t) = S(\vec{r}, t)$$

Where $\Phi(\vec{r}, t)$ is the fluence rate, which can be described as the amount of power incident on a infinitely small sphere at the position $\vec{r}$ normalized by its cross section area. c is the light propagation speed in the material, $S(\vec{r}, t)$ is a source term and D is the diffusion coefficient which reads:

$$D = \frac{c}{3\mu_s'}$$

Taking the wave equation as the starting point, however, has the advantage that interference effects surviving the averaging can be considered, using higher order approximations. Such an effect is enhanced backscattering. For the interested reader there is a short summary of the formal theory in the appendix.

2.3.3 Boundary conditions

The appropriate boundary conditions to the diffusion equation can be shown to be of a mixed type, i.e. combined Dirichlet and Neumann conditions. The boundary conditions are derived by considering the flux of photons traveling through the boundary. The flux is mostly affected by the photon density a couple of mean free paths from the surface, so a valid approximation for the photon density for the purpose of finding boundary conditions is to Taylor expand it around the boundary coordinates [6]. By setting the incoming flux equal to the outgoing flux times the reflection coefficient at the surface the boundary condition at the infinite plane $z = 0$ reads:

$$\Phi - z_e \frac{\partial \Phi}{\partial z} = 0$$

Where z_e is:

$$z_e \equiv \frac{\tau_e}{\mu_s'}$$

Where τ_e is a parameter dependent on the reflection coefficient at the boundary, R.

$$z_e \equiv \frac{2}{3\mu_s'} \frac{1+R}{1-R}$$

If the surface is smooth enough the internal reflection can be estimated by using the mean refractive index of the material and integrating the Fresnel reflection coefficient over all angles. Under the assumption that the photon density varies linearly near the boundary, i.e. $\frac{\partial \Phi}{\partial z} = constant$, this boundary condition is equivalent to extrapolating Φ to 0 at a distance z_e from the boundary. This is realized by introducing a mirror source into the model of the infinite space, in such a way that the photon density is guaranteed to be zero at one extrapolation length z_e from the boundary. How this is done exactly depends on the problem formulation.

2.4 Enhanced back scattering

Enhanced back scattering is an interference phenomena visible in the angular resolved intensity distribution of light back scattered from a material containing randomly located scatterers. It manifests itself as a narrow cone shaped intensity profile on top of the incoherently scattered light distribution. In figure 2.2 a schematic illustration of the phenomena can be seen. The red area, which represents the coherently backscattered light, peaks in the exact backscatter angle. The gray area, which represent the incoherently scattered light, has a much slower varying angular dependence.

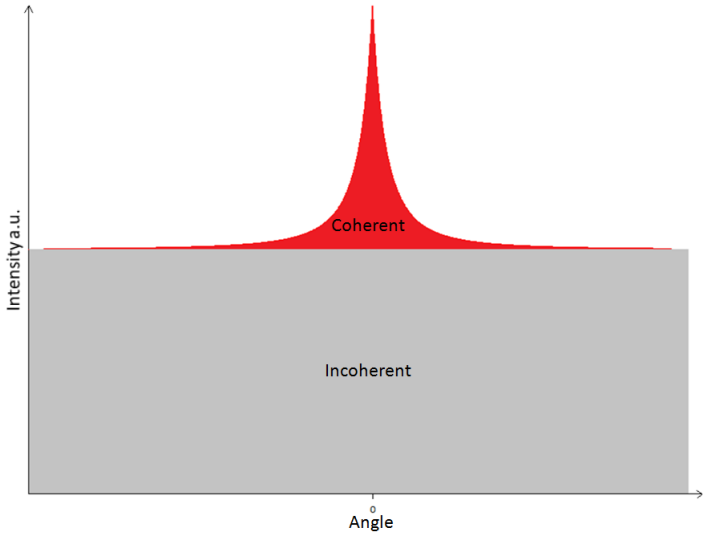

Figure 2.2: *Illustation of the angular resolved intensity distribution of light backscattered from a random material.*

As pointed out earlier, interference effects in the form of speckle is averaged out if multiple sets of scatterer locations are taken in to account. However the mechanisms behind EBS is present independently of the exact location of the scatterers and therefore survives averaging.

To understand this mechanisms, consider the scenario of a light beam impinging on the surface of a scattering random material. The light scattered back through the surface of incidence that have been scattered more than once inside, can be said to have propagated along distinct paths inside the material. These paths can of course also be traveled in the opposite direction, easily seen as a time-reverse invariance of light scattering. Time reverse invariance can be understood as a physical feature of a system where reversing the momentum vectors of the system, i.e. mathematically multiply them by -1, has the same effect as reversing time. In the case of a scattering process this means that a process where a photon traveling from a point A and scatter at a point B to a point C has the exact same probability to occur as if the photon started in C and scattered in B to A.

Each path through the material can thus be said to have a time reverse counterpart with the same probability of being sampled. The light propagating along time reversed paths inside the material have the same optical path length and will enter and exit the surface having the same relative phase. Figure 2.3 illustrates the reasoning for one pair of paths.

The arrows in the figure represents the wave vectors of the incoming light, $\mathbf{k_A}$, and the backscattered light $\mathbf{k_B}$. The black and red lines in between the blue colored scattering centers illustrates the propagation path inside the material. The light traveling along the black path visit the scattering centers in the order S_1, S_2, S_3 and the light traveling along the red path visit the scatterers in the opposite order S_3, S_2, S_1. The red path is thus the time reverse of the black path and the light will enter and exit the surface having the same relative phase. How

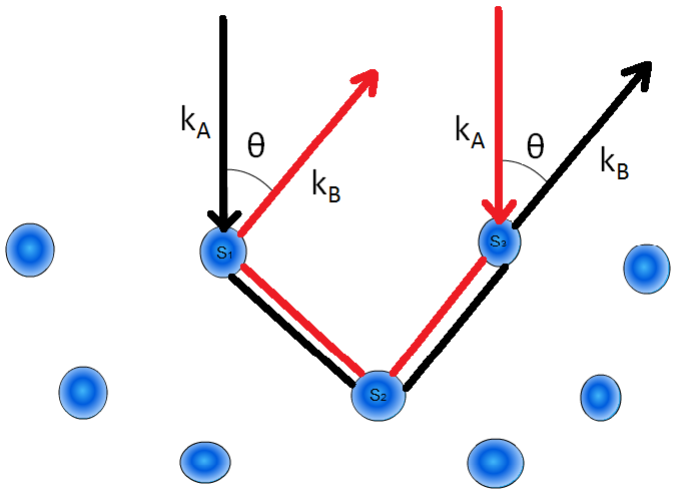

Figure 2.3: *Illustration of the mechanisms behind the EBS phenomena*

the outgoing waves interfere is therefore independent on the actual path, but only depends on the relative location of the first and the last scattering center, $(\mathbf{r_1} - \mathbf{r_3})$ and the angle of observation, θ. In the more general case of course any number, n, of scatterers can be involved. Simple geometrical arguments gives that the phase angle difference $\Delta\phi$ at a point far from the surface is:

$$\Delta\phi = (\mathbf{k_A} + \mathbf{k_B}) \cdot (\mathbf{r_1} - \mathbf{r_n})$$

From this expression it is apparent that in the exact back scattering direction there is no relative phase angle difference, since $\mathbf{k_A} + \mathbf{k_B} = \mathbf{0}$. The interference in this direction is thus fully constructive. If normal incidence is assumed and the first and the last scatterer are approximated to be located in the same plane parallel to the surface plane, a more parsable expression for the phase angle difference can be adopted.

$$\Delta\phi = k_0 \sin(\theta) \, |\mathbf{r_1} - \mathbf{r_n}|$$

Where k_0 is the wave absolute value of the wave vector outside the material. $k_0 \sin(\theta)$ can in turn be seen as the momentum transfer parallel to the surface caused by the scattering, also denoted $q_\perp$.

The EBS phenomena has to be separated from the rest of the interference effects that give rise to speckle. Speckles arise from interference of waves traveling random independent paths. Time reversed paths on the other hand, are not said to be independent.

When calculating the angular resolved ensemble average intensity the electrical field contribution from time reverse paths has to be added up pairwise coherently.

$$\langle I \rangle \propto \left\langle \sum_i E_i \sum_i E_i^* \right\rangle = \left\langle \sum_i E_i E_i^* \right\rangle + \left\langle \sum_i E_i E_{i^*}^* \right\rangle + \underbrace{\left\langle \sum_i \sum_{j \neq i} E_i E_j^* \right\rangle}_{=0}$$

Where $\langle \cdot \rangle$ stands for the ensemble average and I is the angular resolved intensity at an arbitrary point in the backscattering direction. The first term in the resulting sum is the incoherent intensity. The second term is the interference term from time reverse paths. i^* hence denotes the time reverse counterpart of i. The last term is, as before, the interference term form uncorrelated paths, which averages to zero. From one pair of paths the contribution to the angular resolved intensity is proportional to the square of the electrical field plus the interference term.

$$I_i(\theta) \propto E_i^2(1 + \cos(\Delta\phi)) = E_i^2(1 + \cos(k_0 \sin(\theta) \left|\mathbf{r_1} - \mathbf{r_n}\right|))$$

In the exact backscattering direction, the intensity is thus doubled compared to if just the incoherent contributions would be considered. This relation also expresses the translational invariance of the problem. Since the intensity in one angle only depends on the relative distance between the first and the last scatterer, the absolute coordinate system of the surface becomes irrelevant. $|\mathbf{r_1} - \mathbf{r_n}|$ can therefore be replaced by one coordinate r. The total angular resolved coherent intensity can now be expressed as an integral over r, replacing the summation made earlier. The summation indexes then have to be replaced by an r-dependence. $E^2(r)$ is proportional to the incoherent surface distribution $I_{incoh}(r)$, which should be interpreted as the incoherent surface distribution due to a point source in $r = 0$. $I_{incoh}(r)$ in turn is proportional to the total probability for a photon to travel from 0 to r, disregarding interference effects. In integral form the relation can hence be written:

$$I(\theta) \propto \int I_{incoh}(r)dr + \int I_{incoh}(r)\cos(q_\perp r)dr$$

The first term in this relation is the incoherent contribution with no angular dependence, i.e. diffusely scattered. The second term is the coherent contribution which can be interpreted as the Fourier transform of the incoherent surface distribution with regard to the outgoing wave vector. Note that the incoherent intensity distribution is not a real physical quantity but rather alludes to the outcome of models which does not consider coherent wave propagation, e.g. diffusion theory and Monte Carlo simulations.

2.4.1 The physics of the EBS cone shape

The properties of the Fourier transform offers some insight of the EBS dependence on the material properties. If the intensity distribution on the sample surface would be homogeneous and infinitely wide, the intensity distribution in $q_\perp$-space would converge to a delta function. This means that the interference would be destructive in all but the zero angle. A more narrow spatial distribution would, according to Fourier transform theory, give a wider angular

distribution. The spatial intensity distribution depends on the material properties such as scattering and absorption, but also on the geometry of the sample and surface effects.

A high scattering coefficient, μ_s', will yield a wide EBS cone. A photon propagating in the material will then have a high probability of returning to the surface close to the point where it entered. The scattering coefficient is essentially just a scaling factor for the surface intensity distribution. This means that the intensity distribution on a sample surface will have the same shape independent of the scattering coefficient while the scale on the other hand is dependent on the scattering coefficient . The same is true for the angular distribution since the Fourier transform is a linear transformation. This is illustrated in figure 2.4, where the theoretical curve shape, found later in this section, has been plotted for two different values of the reduced scattering coefficient at the same light wavelength.

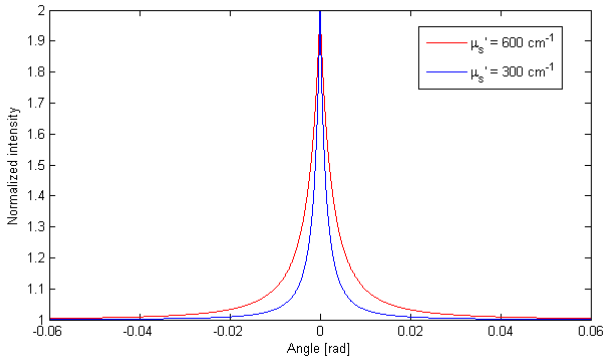

Figure 2.4: *Illustration of how the EBS cone width depend on scattering properties at a light wavelength of 633 nm and no internal reflection*

Absorption will round the peak. This is due to the statistical fact that photons propagation long paths trough the material on average ends up further away from their entry point than photons traveling short paths. They are also more likely to be absorbed. The absorption will therefore mostly effect the edge of the spatial intensity distribution. In the $q_\perp$-space this will lower the high frequency content giving rise the sharp tip of the EBS cone.

Having a thin sample will also round the EBS cone. If photons are allowed to escape through the surface facing away from the incident light, the long photon paths inside the material will be cut of. As in the case with absorption this will mostly effect the the edge of the surface intensity distribution.

Internal reflections occur at the surface of the sample due to refractive index mismatch. An internal reflection has the effect of broadening the surface intensity distribution. When a photon is reflected at the surface it will travel a longer path inside the sample than what it would have done otherwise. This increases the probability for it to escape further away from its entry point. Internal reflection at the interface thus narrows the EBS cone, which is illustrated in figure 2.5. The reflection coefficient (R) is the fraction of the intensity impinging on the surface that gets reflected back into the scattering media.

The conclusion is that it is hard to separate the effects of scattering from

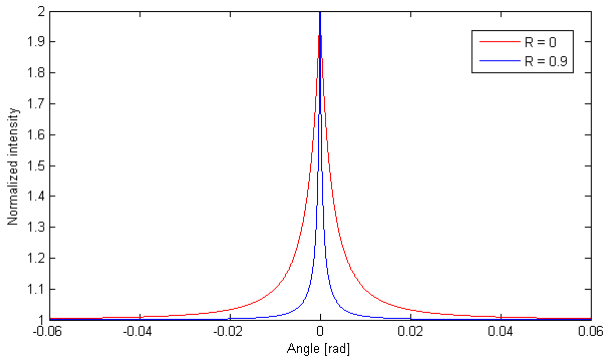

Figure 2.5: *Illustration of how the EBS cone width depend on internal reflection at the material surface.* $\mu_s' = 600cm^{-1}$ *and* $\lambda = 633nm$ *for both curves.*

internal reflection. For any information of the scattering coefficient to be extracted from backscattering measurements the amount of internal reflection at the sample surface has to be measured or estimated.

The model used in this theses for evaluating the experiments on the EBS phenomena does not take into account finite sample thickness. Neither does it account for absorption in the sample. The reliability of the results depended on if these effects can be regarded as negligible. What is accounted for is the rounding and broadening of the EBS cone, due to finite spatial resolution. No optical imaging system can image with infinite sharpness and will therefore act as a low pass filter.

These rather informal arguments are sufficient for good physical understanding of the mechanisms giving rise to EBS. However, it is a rather crude model to assume that all intensity is scattered out from the surface in the same plane. Furthermore it is not completely true that the incoherent intensity distribution is angular independent in the backscattering direction, since internal reflection at the surface introduces a slight angular dependence. In the appendix the main features of a much more formal and rigorous approach, with the power to make quantitative predictions, is presented. The main result, an analytical expression for the EBS cone curve shape, is however cited here as well for the sake of completeness.

The angular dependence of the backscattered light is expressed in terms of the bistatic coefficient (γ). This is the backscattered intensity normalized to the incoming intensity (I_0), the area of observation ($A\cos(\theta_i)$) and distance of observation (r), where θ_i is the angle of incidence. The bistatic coefficient is defined as:

$$\gamma \equiv \frac{4\pi r^2}{I_0 A \cos\theta_i}$$

The bistatic coefficient for the coherently backscattered light (γ_c) can according to [5], if the light can be approximated to be scattered from a semi infinite space, be described by:

$$\gamma_c = \frac{3}{2v\cos\theta_i}\frac{1}{(\alpha+v)^2+u^2}\left(1+\frac{2v\tau_e}{1+\tau_e\alpha}\right)$$

Where the following definitions has been made:

$$u \equiv \frac{k_0}{\mu_s'} \left(\cos\theta_i - \cos\theta_s\right)$$

$$v \equiv \frac{1}{2}\left(\frac{1}{\cos\theta_s} + \frac{1}{\cos\theta_i}\right)$$

$$\alpha \equiv \frac{q_\perp}{\mu_s'}$$

Where θ_s is the scattering angle. The parameter τ_e is known as the extrapolation ratio and its value depend on how much light that gets internally reflected at the interface.

Chapter 3

Setup

This chapter will introduce and describe the setup for measuring enhanced backscattering in highly scattering media, constructed in this project. The different components in the setup will be explained in detail. The problems regarding the system will be highlighted, both the practical problems and the experimental difficulties during the project will be commented.

3.1 Overview

The EBS setup is founded on the principle of measuring the angular resolved backscattering. The basic idea is to let the light be transmitted through the beamsplitter onto the sample and to let the backscattered light be reflected by the beamsplitter towards the detector. A schematic figure of the system is shown in figure 3.1. The lenses are all placed in holders for a optomechanical micro system with metal rods to hold it in place. In some of the measurements the sample holder and the DC-rotational motor is exchanged with a mirror. Adjustable neutral density filters are placed right after the light source in order be able to suppress more light when the mirror is inserted in the setup than for a scattering sample. In the following sections the components will be described in more detail. The most advantageous property of the setup is that it is a fixed setup with no moving parts, except for the rotating sample. It was mainly the practical aspect of the system that supported this particular setup, since it is relatively easy to build and still have a good angular resolution. In this setup the detected angular range is around 60 mrad and the estimated angular resolution is about 0.26 mrad.

3.2 Source

The light source in the setup is a 10mW HeNe laser with the wavelength of 632.8 nm, model 1125/P Uniphase. All the optical component are all placed onto an optical rail in order to maintain alignment of the optics. Two positive lenses are placed after the source, the first lens is used to expand the beam and the other to collimate the expanded beam. The beam is expanded roughly 10 times to minimize the divergence.

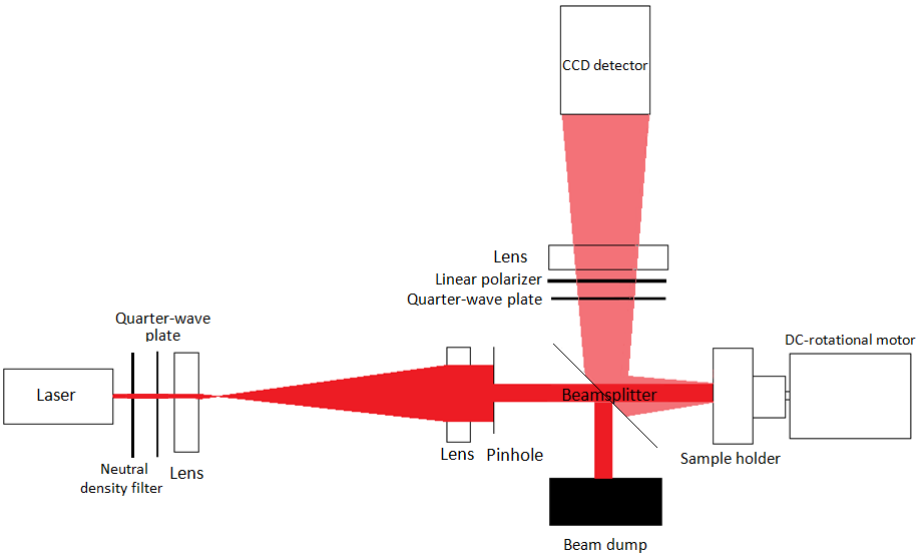

Figure 3.1: *The EBS setup*

3.3 Imaging

The imaging lens is placed as the last optical component in front of the detector and will focus the light onto the detector. The rays that are parallel with each other will be focused in the same spot as seen in figure 3.2. The lens will hence image the distribution of spatial frequencies on the CCD-chip.

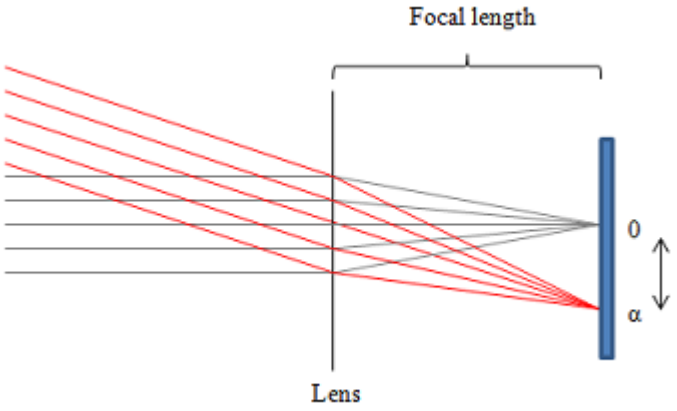

Figure 3.2: *The figure illustrates the lens will focus the parallel light from different angles.*

As a detector it is possible to choose both a point detector (e.g. PMT or photodiode) or a CCD detector. [7][8]. A CCD-camera has been chosen for this setup, since it enables the system to be fixed and makes it possible to not have to translate the detection part of the system when measuring. Additionally it

will simplify the capturing of the data and a lot more data will be recorded in one recording and therefore decrease the time of the measurements. The camera, Hamamatsu, model ORCA-AG is a high resolution cooled CCD digital camera with a 12-bit dynamic range. The maximal angular range measured is dependent on the focal length of the last lens. A long focal length will image a smaller angular range and will give a higher resolution of the backscatter cone. Several trials were made to image the angular resolved reflectance with lens objectives. All trials resulted with problems in getting the whole area of the CCD-chip illuminated. The solution was to operate the camera without its lens objective. A single lens is used to image the light, instead of a complex system of lenses. This brought about another problem, dust on the sensor cover glass. Dust particles are drawn towards the sensor when the camera is running due to the charges in the CCD. In figure 3.3 dust spots can be seen in the images. The CCD camera has a cover in front of the CCD chip in order to protect it. When tilting the camera slightly back and forth it can be seen as the "dust" is moving on the screen and that is due to that the cover is not placed precisely at the surface of the sensor. Images that will look like this with that same type of spots is probably due to dust. The dust could be temporarily removed with pressurized air.

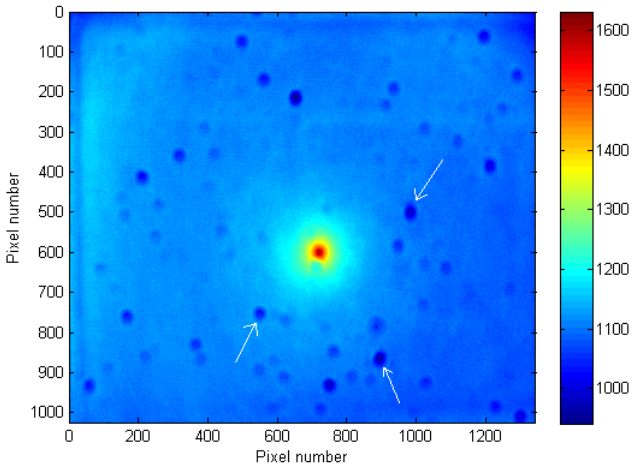

Figure 3.3: *The figure displays dust spots on the camera, some of the spots are marked with an arrow.*

Dust settles rather quickly on the camera when used without an objective lens. It is a good idea to protect the camera with a lens cap in between measurements.

Some other problems with the camera have been spotted, the border of the sensor does not seem to cool effectively while it is illuminated leading to a higher photon counts than what is true. To see that, a lens cap was put in front of the camera blocking all other light and from a "'dark frame"'. It was possible to see a inhomogeneous distribution of noise along one of the borders before it

was cooled down, see figure 3.4.

Another camera, model CV-M10 SX from Jai, was tested in order to determine if the unexpected inhomogeneous background, that can be seen in the measurements for the averaged EBS-measurement, was due to the ORCA-AG camera. It was possible to detect some uneven distribution over the image, even here. This indicates that the uneven distribution depends on some optical effect and not the camera. The ORCA-AG camera gave better images due to a wider dynamic range and was easier to handle, so this camera was used under the remainder of the project.

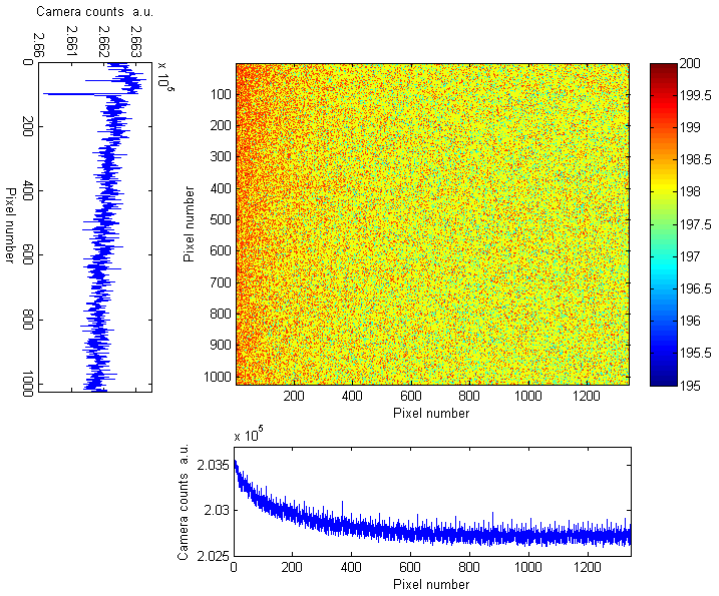

Figure 3.4: *Displays the camera distribution of a dark frame. The plots on the left and below the picture is a summation of the rows and columns respectively and illustrates the uneven distribution.*

3.4 Beamsplitter

The beamsplitter has created some problems during the project. The first beamsplitter that was used did not have any specification of the its properties. When the coherent backscattering was clearly imaged onto the detector and sufficient contrast had been obtained, it was noticed that a multiple of lines ran through the captured images. The lines were very narrow and looked very straight. It was discussed whether these lines depended on the read-out of the camera or was an interference effect. The lines did not follow the rows of the pixels and it could be concluded that the effect was due to interference. The beamsplitter was thus considered to be the most probable candidate to give rise to the interference. The thickness of the beamsplitter was estimated and a rough model was created to explore if the beamsplitter could create such a pattern. Figure 3.5 shows the interference pattern for the beamsplitter on the left and on the right

is the modeled interference. As can be seen from figure 3.5 the measurement coincide rather well with the model.

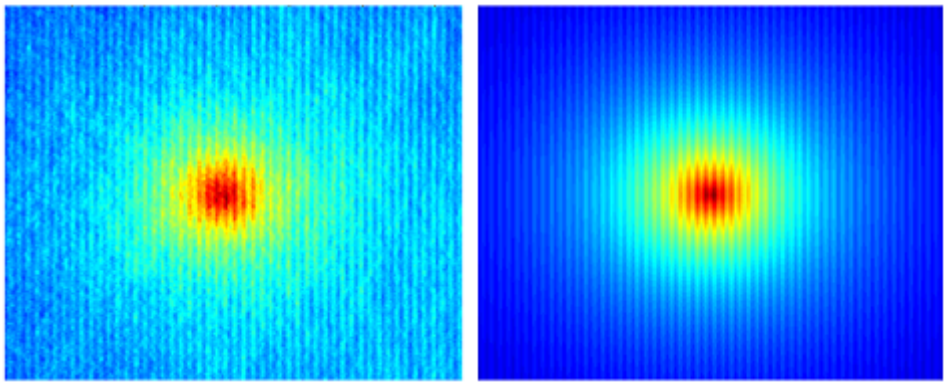

Figure 3.5: *To the left is the measured image that displays the interference pattern. At the right is a model of the interference pattern, where the thickness of the beamsplitter was estimated, multiplied with the theoretical curve as a small disturbance.*

In thin layers, light that is reflected in both the front and back surface will interfere. The Fresnel equations can be used in order to determine how much of the light that is reflected in the surfaces. The spatial frequency of the interference fringes is dependent on the thickness of the layer and the angle of observation.

In order to avoid problems due to interference effects certain properties of the beamsplitter needed to be fulfilled.

- Thick glass plate
- Anti reflection coating
- Wedge

It is preferable to have a thick component because the fringes will be broader. Anti reflection coating will reduce the reflected light from 4 % to less than 1 % and will reduce the light interaction between the light reflected in the front and back surface and therefore reduce the interference effects. An additional feature is that a small wedge is introduced to misdirect unwanted reflections. The old beamsplitter was replaced with a new one with better properties than the last. The aquired beamsplitter has a diameter of 1", a thickness of 5 mm and it has a wedge of 30 arcmin, which in degrees corresponds to one half degree. It is a UV Fused Silica Broadband Plate Beamsplitter with coating from 400-700 nm intended for an incident angle of 45°, from Thorlabs. Another idea is to use a beamsplitter cube, however this approach has a problem with reflections at the cube' surfaces that will be directed towards the camera. Even though the acquired beamsplitter was antireflection coated it still created a weak reflection in the back surface (ghosting) that can be see in the IRF measurement. However the ghosting has a large angle, about 0.5°, to the exact backscattering direction (zero angle) because of the wedge and will probable not influence the results.

3.5 Polarization optics

The intensity of the backscattering at zero angle should be twice that of the incoherent background. Experimentally however this is not always the case. The enhancement factor is defined as the ratio between the intensity at exact backscattering angle and the incoherent background level. The detection of photons only scattered once in the sample, single scattered light, will reduce the enhancement factor. The path of a single scattered photon can have no time-reverse. These will hence not contribute to the coherently backscattered light but only add to the incoherent background. In order to reduce the single scattered light polarization optics have been used.

A quarter-wave plate converts linear polarized light into circular polarized light. Light moving towards the sample will be circular polarized. The photons that will only scatter once in the media, the single scattered light, will flip its helicity. A flip in helicity means that it changes its polarization state from e.g. right to left polarized light. The multiple scattered light will on the other hand lose its polarization. The backscattered light is converted back to linear polarized light by the quarter-wave plate on the detection side and can thus be blocked by a linear polarization filter. Hence, it is possible to block the single scattered light due to the flip in helicity. This is called detection in the helicity preserved channel.

Another reason for the incident light to be circular polarized is, because it is circular symmetric. The symmetry of the backscattering is dependent on the polarization of the incident light and the light let through to the detector [9]. Linearly polarized light can show a bias in its backscattering direction due to anisotropy in the first few scattering events. This effect was investigated in [10] by Monte Carlo simulation of polarized multiple Mie scattered light. To avoid anisotropic effects circular polarized light is used.

Usually this type of setup contains only one quarter-wave plate placed between the beamsplitter and the sample as in [7]. This configuration was tested, however, the quarter-wave plate needed to be rotated in a relatively large angle in order to ensure that the back reflection in the surface did not hit the detector. It was uncertain how the angling of the polarization plate affected the performance, so instead two quarter-wave plates were used as in [11]. The light from the laser was then not directly reflected towards the detector. As seen in figure 3.1 the beam passed the first quarter-wave plate before the beam was expanded and the second one was placed right after the light was reflected in the beamsplitter. The first polarization plate was a polymer quarter-wave retarder film from Edmund Optics. The second quarter-wave plate was a mounted achromatic polarization plate of crystalline quartz and magnesium fluoride for the wavelength range 450-800nm and the diameter of the plate was 9 mm from Thorlabs. The linear polarizer film was from Edmund Optics.

3.6 Sample holder and DC rotational motor

The sample used during the setup had a diameter of 13 mm. The samples needs to be exchangeable in the holder and it might be of interest to be able to measure samples of different thicknesses. To fulfill those demands a sample holder was designed as follows, see figure 3.6. To ensure the ability to exchange

samples a hose clamp was used to securely fastened the sample in the sample holder. The current hose clamp is a bit unwieldy and it would advantageous to find another way to make it easier to fasten the sample.

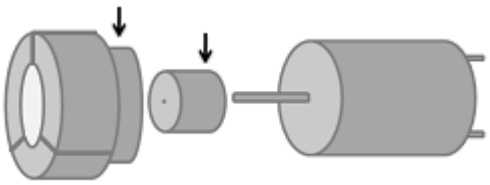

Figure 3.6: *In order for the sampleholder to rotate, it needs to be attached to the DC-rotational motor with interconnectors. The motor has a shaft with a diameter of 2 mm. The hose clamp is not visualized.*

Due to the high spatial coherence of the light source, a speckle pattern occurs which needs to be averaged out. This is done by placing the sample holder on a rotational DC-motor. The rotation axis is the same as the propagation axis of the light. But this is not sufficient to completely average the speckles out, the sample also needs a vibrational movement in order to eliminate speckles completely. The rotation pattern can be seen in figure 3.7 The vibrations are induced by the fact that the load on the rotational motor is not evenly distributed. And further enhanced by placing the holder on an elastic adhesive compound, Blu-Tack, because this created adequate vibration.

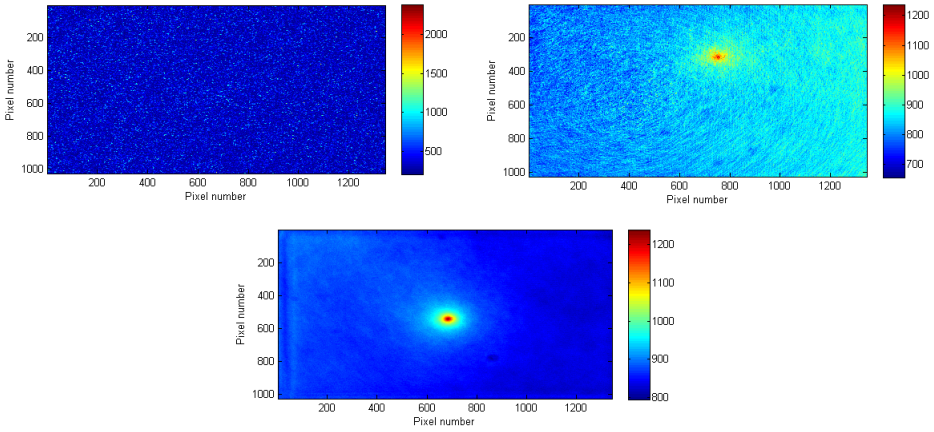

Figure 3.7: *Three images of the enhanced backscattering. The image on the left top is not at all averaged and will therefore only show the speckle pattern. The image on the right top is rotated in order to average out the speckle pattern, but it is not successful since a rotation pattern is visible. The bottom image visualizes the average enhanced backscattering. For this measurement the sample has both been vibrated and rotated.*

Chapter 4

Measurements and Data Analysis

4.1 Measurements

In this chapter the measurements are described. All the measurements were performed on a sample consisting of TiO_2 in epoxy with a diameter of 13 mm and a thickness of 4 mm. The measurements are described in more detail in the following sections. For the measurements mentioned below different settings on the neutral density filter are utilized in order to block different amounts of light. In order to measure the instrumental response function and in order to calibrate the angles, the sample is exchanged with a mirror. The neutral density filters is set so that only a small fraction of the light is transmitted when the light is reflected on a mirror, otherwise there is danger of damaging the sensor on the CCD-chip. In order to determine values for the reduced scattering coefficient a series of different measurements is needed apart from the enhanced backscattering measurement. It is necessary to calibrate the angles and this was done by illuminating a grating with parallel light. An instrumental response function is measured in order to compensate for the finite resolution and instrumental imperfections like the alignment of the optics. Then the actual EBS measurement was carried out and a background measurement was acquired. Finally a measurement of the sample illuminated from the back with a light emitting diode is carried out. The image acquisition software used for the Hamamatsu camera is called Wasabi. In order to acquire the best signal-to-noise the acquisition software's ability to average a multiple number of pictures was used. The intensity of the laser and the exposure time of the camera have to be balanced in order to make use of the entire dynamic range.

4.1.1 Instrument response function

The reason for measuring the instrument response function, IRF, is to compensate for the divergence of the source, finite resolution of the lens and other imperfections in the optical system. This is done by removing the sample and letting the light fall onto a mirror. The mirror is adjusted so that the incident light is perpendicular to the surface of the mirror and the light will be reflected

back in incident angle. The positive lens on the detection side will focus the parallel beam into a point on the CCD detector. If the point on the CCD detector is small and has a circular shape it is an indication that there is no obvious problem with the optical system. The lens is adjusted so the IRF becomes as small as possible. It is important to remember that it is just a compensation for the finite resolution but can not be seen as a correction for the reflectance characteristics for the beamsplitter.

4.1.2 Angle calibration

In order to determine how the pixels of the camera corresponds to angles, the distance between the lens and the CCD chip needs to be determined accurately. A transmission grating with 10 lines/mm was used in order to calibrate the angles. In order to view the Fraunhofer diffraction for a slit the detector needs to be placed far away from the slit. Even if the detector is in the vicinity of the grating it is possible to calibrated the angle this way, due to that the light will propagate through a converging lens. The lens will focus the interference pattern onto the detector at its focal plane. The distances between the interference maxima can be found out by images from the CCD camera. From the grating equation the angles can then be calibrated. The grating equation is written below where d is the distance between the slits, m the order of the intensity maxima and θ is the angle of the intensity maxima

$$d \sin\theta = m\lambda \qquad m = 0, \pm 1, \pm 2, \ldots$$

4.1.3 Sample measurements

Due to the fact that the sample is constantly rotated during the recordings in order to average out the speckles, it is not advantageous for the laser to fall onto the center of rotation, since it will not move as much and there will be less averaging. Considering this, the sample is placed in a position where the light spot is somewhere between the middle of the sample and the outskirts of the sample. For every EBS measurement a background measurement needs to be acquired with the same exposure time.

4.1.4 Angular transmission characteristics

In an effort to make a flat field compensation for any unevenness in the spatial sensitivity map, a measurement with a sample illuminated from the back was made. It is assumed that the transmitted light is diffuse with small or no angular dependence. This measurement should be done when the sample is situated at the same distance from the detector as in the EBS measurement. The LED has a center wavelength of 630 nm. Speckles will not occur from a transmission measurement with an LED, as the coherence length of that light is too short for generating any speckles. To be able to receive the same background distribution as for the EBS measurements, the light will only be allowed to leave the area that was illuminated with the laser in the EBS measurement. This measurement should also help to account for the dust particles that were not possible to remove with pressurized air.

4.2 Data Analysis

In order to determine the reduced scattering coefficient the theoretical model of the enhanced backscattering needs to be fitted to the measurements. Figure 4.1 is a schematic illustration of the different steps in the data processing. All the data processing of the images and the evaluation have been performed in MatLab.

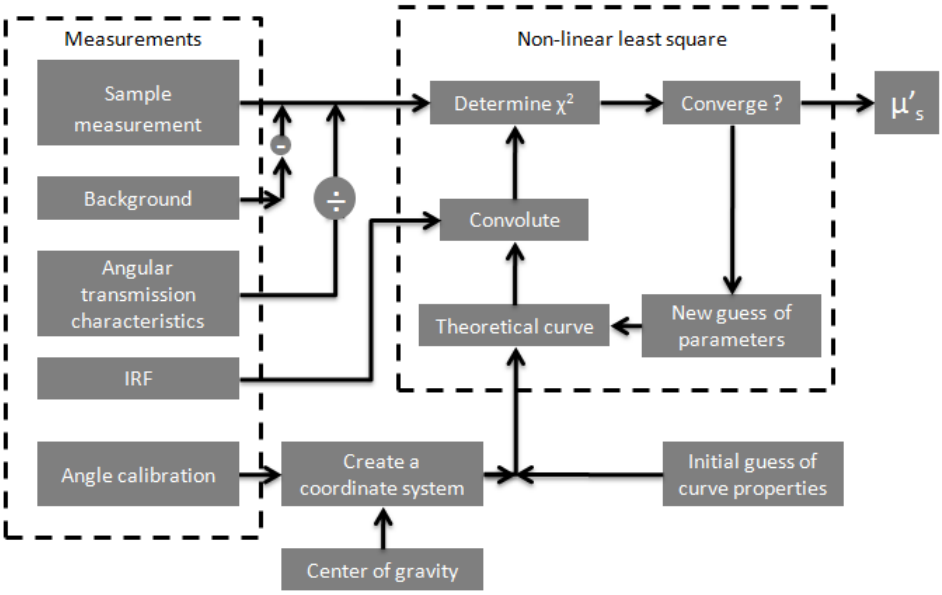

Figure 4.1: A schematic illustration of the evaluation

One of the considerations of the evaluations have been how to treat the data. In the initial stages the data was evaluated using just one pixel row or column in order to investigate whether the data could be well described by the model. Because a CCD-camera is used as a detector, it is of course more advantageous to analyze all the data in the entire image plane. This can be done in two ways. Either by fitting the model to all the data points in the image grid (full grid), or by averaging the intensity over all azimuthal angles and thereafter do the fit (averaged data).

4.2.1 Data processing of measurements

In order to fit the measurements and the theoretical curve to each other, the data from the measurements needs to be processed. The background is subtracted from the sample measurements. The sample measurement is divided with the normalized transmission characteristic measurements, see figure 4.1. From the angle calibration measurement a script has been constructed to create a coordinate system, according to the grating equations, see section 4.1.2. This coordinate system is adjusted so that the zero polar angle coincides with the center of the EBS cone in the image from the measurements.

4.2.2 Finding the exact backscattering direction

One of the main issues in order to interpret the measurements has been to locate the center of the EBS cone. Different strategies have been incorporated. These have been to set the exact backscattering direction as the maximum intensity of the IRF, the maximum intensity of the sample measurements or to make an initial guess and set the exact backscattering direction as a parameter to be evaluated. However, calculating the center of gravity of the EBS-cone seem to be a good way to find its center.

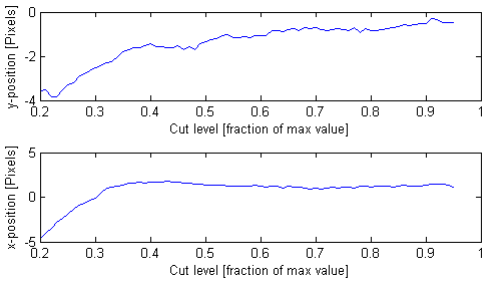

Figure 4.2: *Center of gravity of the EBS cone as a function of cut of fraction.*

Figure 4.2 shows an example of the result from a center of gravity calculation as a function of the fraction of the cone height that is taken into consideration. Thus a fraction of e.g. 0.5 means that the cone is cut off at half its maximum value and the center of gravity of the upper part is calculated. The coordinate system is shifted so that the zero angle coincides with the center of gravity, according to the values displayed on the y-axis in the figure. These plots indicate that the method is somewhat unstable but still it is less arbitrary than just placing origo at the maximum value. In the data analysis a cut of fraction of 0.5 was used. If the peak is cut at a level too close to the baseline level the method doesn't work since the baseline has a gradient which slightly distorts the base of the cone.

4.2.3 Evaluation of the reduced scattering coefficient

There are three different parameters (μ_s', C, S) evaluated in the data fitting. μ_s' is as mentioned before the reduced scattering coefficient. C is a constant that gives the level of the background. The third parameter S is a scale factor that is adjusted to the measurements.

An initial guess of these parameters is sent into the non-linear curve fit. One or two extra variables could in addition be incorporated in order to be able to translate the curve in x- and y- direction. Apart from these initial guesses, it is necessary to insert the refractive index of the sample. The refractive index is used to calculate the reflections coefficient of the sample from the Fresnel equations. It is assumed that the surface of the sample is sufficiently smooth to utilize those equations. When the reflection coefficient is determined, the extrapolation ratio, see section 2.3.3, can be inserted into the theoretical model. The theoretical curve is then convoluted with the IRF in order to compensate for the broadening of the measurements.

The curve fitting is performed through successive iteration using non-linear least squares method according to the Levenberg-Marquardt algorithm. The least squares method means that the function χ^2 is minimized with respect to the parameter values, $\mathbf{p}$.

$$\chi^2(\mathbf{p}) = \sum_{i=1}^{m} \frac{(y_i - f(x_i, \mathbf{p}))^2}{w_i^2}$$

Where y_i is the values of the measurements and $f(x_i)$ is the model function value at x_i. m is the number of data points and w_i is the weight put at each sample point.

If the difference is small enough to reach a preset tolerance value then the evaluation is complete and the reduced scattering coefficient is extracted. Otherwise a new guess of the three parameters is evaluated. The terms in the χ^2 function are weighted by the number of sample points at the azimuthal angle of each data point. Most emphasize will be put on the measuring point of the exact backscattering direction, since there is only one sample point for the exact backscattering direction.

Chapter 5

Results

In this chapter the results from the measurements, carried out on a phantom tablet of TiO_2 in epoxy using the experimental setup, will be reported. The purpose of presenting these results is to show the performance of the system.

5.1 Results from measurements

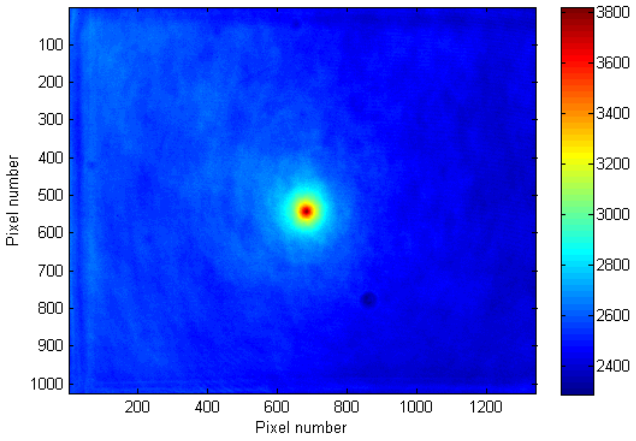

Figure 5.1: *Raw data image of enhanced back scattering. The bar on the right side indicates how the color scale translates into camera counts.*

In figure 5.1 a raw data image acquired by the system is displayed. The bright structure in the center of the image is the characteristic cone from the coherently backscattered light. The image is an average of 150 pictures each captured with an exposure time of 100 ms. Despite the averaging some residues from the speckle remain in the form of a rotation pattern. There also seems to be an intensity gradient from the right to the left in the image. Along the upper, lower and the left edges some kind of structures resulting from instrumental flaws are visible. The dark circle in the lower right part at 5 o'clock of the image is a dust spot on the sensor protective glass.

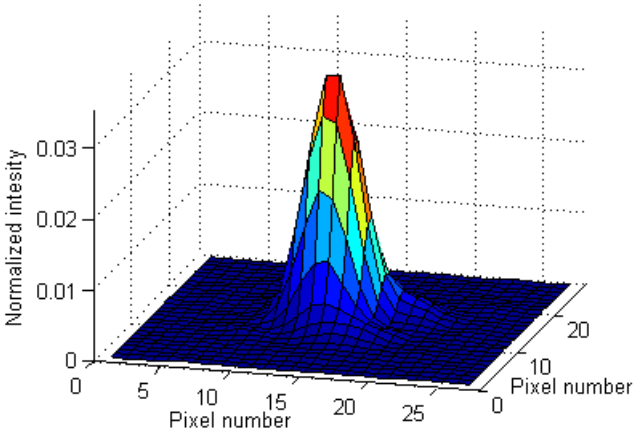

Figure 5.2: *Surface plot over the instrumental response function*

Figure 5.2 displays the instrumental response function used for the evaluations reported later on in this chapter. The FWHM of the IRF was estimated over its widest part. This gives an approximative measure of the instrumental angular resolution. In the series of measurements presented here the estimated angular resolution is 0.258 mrad. This could be compared to the EBS cone's expected FWHM of approximately 2.5 mrad. The convolution between the IRF and the data image leads to loss of information at the image edges. In this case about 3% of the total information is lost due to the convolution.

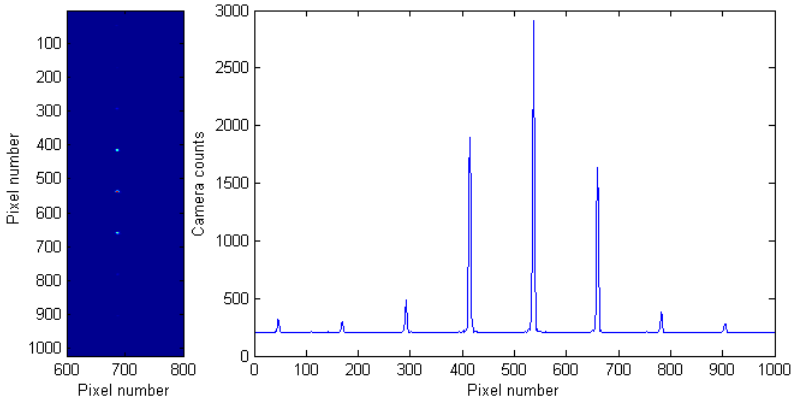

Figure 5.3: *The picture to the left is a cropped image of the diffraction pattern from the grating on the camera CCD-chip. To the right is a cross-section along the intensity maxima from the left picture.*

Using the image in figure 5.3 and grating equation the distance from the lens to the CCD-chip is determined to 12.5 cm. The angular separation between the 0:th and first order maxima is 6.3 mrad. The total angular span in the raw data images is approximately 70 mrad horizontally and 50 mrad vertically.

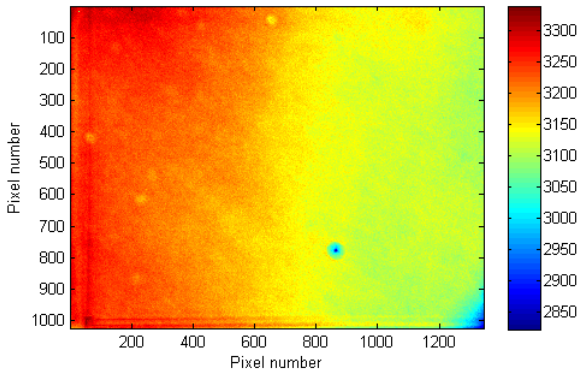

Figure 5.4: *The distribution of light on the CCD-chip from a LED trans illuminated sample.*

Figure 5.4 displays the intensity distribution at the CCD-chip from a LED transilluminated sample, i.e. the transmission characteristic measurement. The image was acquired from averaging over 100 frames, each taken with an exposure time of 10 s. Just as in figure 5.1 there is an intensity gradient from the right to the left in this image. The gradient yields a difference of about 5% between the extremes. In the ideal case the distribution of the disperse light should be even. Hence the image indicates that the transmission characteristics of the system is not the same for all angles.

5.2 Results from data analysis

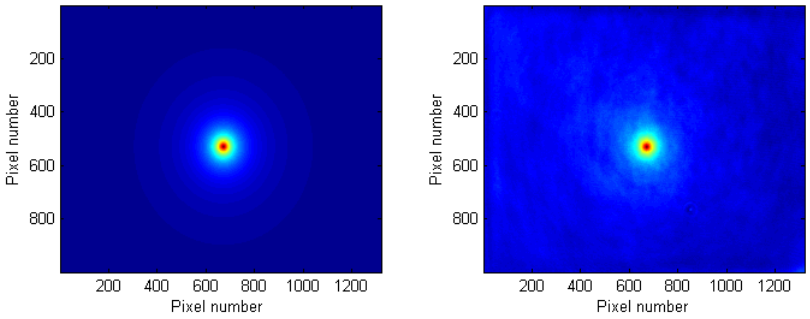

Figure 5.5: *The image to the left is the theoretical curve shape fitted to the measurement which is in the image to the right*

Figure 5.5 displays the result of the evaluation of the EBS curve shape together with the original data image which is compensated for the transmission characteristics of the system. The extrapolation ratio was chosen such that it would correspond to a refractive index mismatch of 1.5 at the interface. This choice is motivated by the fact that the refractive index of epoxy, which is the main constituent of the phantom, is about 1.5. In this evaluation the theorthical

curve is fitted to all the data points in the image grid. The residual from the fit is displayed in figure 5.6. Apparently there are systematic deviations in the experimental data that the model does not account for. The residual should be completely random, which is not the case. The top of the cone can be distinguished in the residual as well as a gradient from left to right. The gradient in the residual means that the data fitting routine has a problem with finding a proper baseline level even though the transmission characteristics has been corrected for. This problem can be seen in the cross-section plots in figure 5.7. The baseline level, even though it is not an interesting parameter in it self, is important in order to get a correct estimation of the curve width. Still, disregarding the anomalies the theoretical curve shape seem to describe the data quite well for small angles.

Theoretically the cone's peak intensity should be twice the intensity of background. The fraction between these intensities is referred to as the enhancement factor. In the measurements presented here the enhancement factor only reaches 1.6 and not the theoretical level of two.

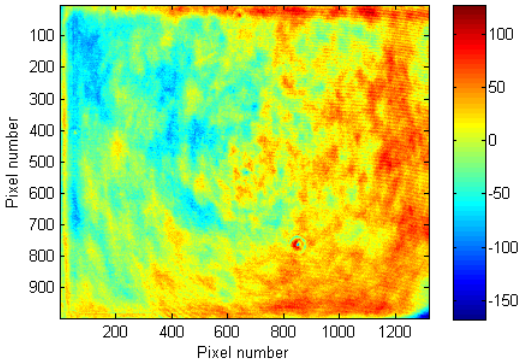

Figure 5.6: *Residual from data fit.*

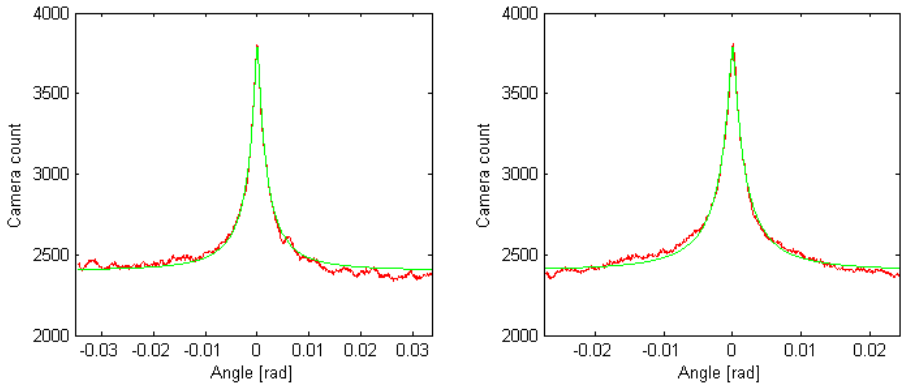

Figure 5.7: *Vertical (right) and horizontal (left) crossection of the EBS-cone, measurement data (red) and fitted curve (green)*

Another method for evaluating the data is to fit the theoretical curve shape to the average intensity over all azimuthal angles. This approach is illustrated in figure 5.8. The result should be equivalent in terms of estimated parameter values, but since the statistical deviations are averaged out the result can be easier to visually interpret. In this case both evaluations tend to be poor in the same angular range, i.e. at angels larger than 5 mrad.

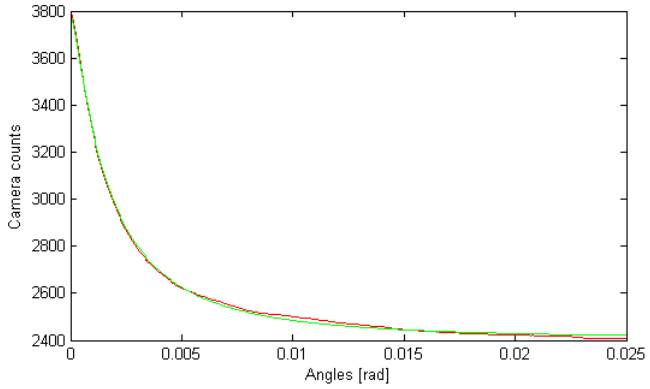

Figure 5.8: *Data averaged over all azimuthal angles (red) and fitted theoretical curve (green)*

In order to get a sense of the performance stability of the optical arrangement and evaluation, five measurements were made under the same conditions and evaluated using the preferred evaluation method. The results of these study are presented in 5.1. The estimated reduced scattering coefficients seems to be rather stable apart from the deviant value from measurement 2. This deviation could probably partly be explained by the fact that the dynamic range of the camera was not utilized in the same extent as for the other measurements.

Measurement	1	2	3	4	5
μ_s' $[cm^{-1}]$	637	669	639	634	632

Table 5.1: *Comparison of five successive measurements on the same sample*

5.3 Comparison with TOFS results

The reduced scattering coefficient of the current sample was measured by the time-of-flight spectroscopy (TOFS) instrument at 633 nm, in order to give a reference value for the EBS measurements. This is a time resolved technique where the diffusion coefficient is estimated from the distribution of flight time of photons transmitted through the sample [1]. The reduced scattering coefficient can be extracted from the diffusion coefficient, see section 2.3.2. In table 5.2 the reduced scattering coefficients are displayed evaluated with two different measuring techniques, EBS and TOFS. The EBS measurement data analysis is conducted using both the full grid and the average method. All three methods should of course give the same value of the reduced scattering coefficient. The

first two values in table 5.2 originates from the same data and the difference in the values must thus be consequence of the evaluation methods.

Method	μ_s' [cm^{-1}]
EBS - full grid	637
EBS - averaged data	627
TOFS	575

Table 5.2: *Estimated reduced scattering coefficient of the sample at the wavelength 633 nm using two different techniques. The refractive index of the sample was taken to be 1.5.*

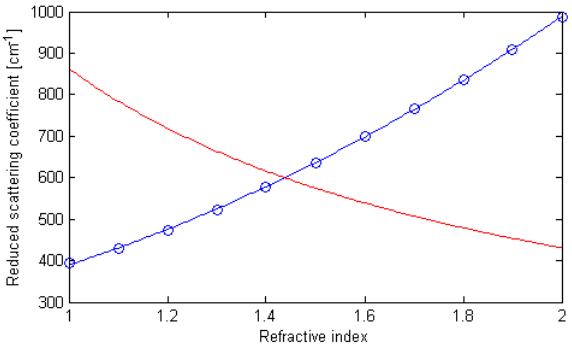

Figure 5.9: *The red curve is the estimated reduced scattering coefficient as a function of refractive index calculated from the time dependent diffusion coefficient measured by TOFS. The blue curve is a second order polynomial fitted to estimations of the reduced scattering coefficient made from a EBS measurement for different refractive index.*

Figure 5.9 provides a comparison between estimations of the reduced scattering coefficient for the same sample made by a TOFS (red) and an EBS measurement (blue). The diffusion coefficient depends on the effective refractive index of the scattering media and hence the estimation of the reduced scattering coefficient extracted from the TOFS measurement is dependent upon what refractive index is plugged in to the evaluation model. The TOFS curve has the form:

$$\mu_s' = \frac{c}{3nD_0}$$

D_0 is the diffusion coefficient estimated from a TOFS measurement at a light wavelength of 633 nm and where the sample is assumed to have a refractive index of 1.5. n is the effective refractive index. The blue curve has been produced by taking one set of EBS measurements and varying the refractive index put into the model. Varying the refractive index put into the model is equivalent to varying the extrapolation length in the boundary condition of the diffusion equation. The physical effect causing the variation in the estimation of the reduced scattering coefficient is not the same for the two methods. In the case of TOFS, the refractive index describes the light propagation speed in the

sample, while in the EBS model it describes the boundary conditions and the amount of internal reflection taking place at the interface. The plot indicates that the refractive index of the sample should be about 1.44, corresponding to an internal reflection coefficient of 0.49. The sample consists of epoxy with an refractive index of about 1.55 and TiO_2 with a refractive index of about 2.5. It seems unlikely that the refractive index of the compound would be lower than those of its separate constituents.

Chapter 6

Discussion and conclusion

The goal for this work has been to investigate the possibilities of measuring the reduced scattering coefficient in a highly scattering random material by utilizing the EBS phenomena in steady state. During this project it has been seen that it is easy to detect the EBS phenomena in a simple setup with quite few optical components. It has, however, proved rather more difficult to image the backscattering with sufficient quality for accurate extraction of the reduced scattering coefficient.

Despite the somewhat relatively poor imaging quality, the method still proved to produce fairly reproducible values of the estimated scattering coefficient. The system has, however, so far only been tested on one sample and therefore it is difficult to say much about the overall stability of the system. Even if the system proves to be stable when measuring on samples with different scattering properties, the accuracies of the values need to be validated.

The data from the measurements were analyzed in two different modes, the *full grid method* and the *average data method*. Since it is much easier to detect anomalities in the data and in the fit using the full grid method, this evaluation method is preferable to the average data method.

In an effort to try to estimate the performance of the system, the same sample was also measured on by the TOFS-system and the result was compared to the EBS measurement. Since TOFS is a well established method of measuring the reduced scattering coefficient, it was used as a standard of comparison. The estimation of the reduced scattering coefficient differs for the two measuring techniques when assuming the same refractive index, see table 5.2. Unfortunately the estimation of the reduced scattering coefficient using the EBS-system is very sensitive to the selected boundary conditions. In the current model the boundary condition is solely dependent on the effective refractive index of the material. Likewise, the evaluation of the TOFS data is dependent upon the refractive index. The hope was therefore to be able to extract the refractive index from a comparison between the result from the two measurements. This comparison resulted in an unreasonably low estimation of the refractive index. This fact suggests that the validity of in the results from the EBS-measurements is somewhat dubious.

There can be two main reasons why the estimation of the reduced scattering coefficient doesn't give a result closer to the estimated value, bad data quality and model flaws.

There obviously is a challenge to obtain sufficiently good data quality at large angles in the EBS images, resulting in an uncertain estimation of the baseline level. These anomalities were expected to depend on the transmission characteristics of the setup. The intention was to compensate for this by an image of the angular distribution of the light from a trans illumination of the sample by incoherent light. The strategy was not fully successful, even though the gradient in the background level was decreased, it was not completely removed. The result of the evaluation showed to be sensitive to variations in the baseline level. The most reliable way to get around this problem is probably to measure the incoherent background level independently, i.e. at large enough angles far away from the backscattering cone. In practical terms this means that the set up most likely needs a rotating part [12] [11], alternatively a curved array of detectors [13].

The quality of the measurements also suffered from the small size of the imaging optics. The most limiting components was the quarter wave plate in front of the imaging lens, which had a diameter of only 9 mm and the one inch circular beamsplitter which put at an angle of 45° created a elliptical projected area with a short half axis of 8.67 mm. A rough calculation yields that, given the dimensions of the set up, the limitations would allow for imaging of an angular span of $\pm 4°$, under the condition that all the components were perfectly aligned and that the illuminated spot on the sample was 3 mm in diameter. Larger sized optical components would allow for a larger beam diameter, decreasing the divergence of the illumination and consequently increase the angular resolution. For the purpose of measuring samples with a reduced scattering coefficient in the range of 600 cm^{-1} the angular range of $\pm 4°$ was sufficient. The measurements were, however, quite sensitive to small misalignments.

Another important reason to why the estimation of reduced scattering coefficient does not give a valid result is probably the method used for determinening the boundary conditions. As pointed out before, the estimation of the reflection coefficient at the boundary obtained by using the Fresnel's law may not be valid since the roughness of the surface might be too coarse. Still this was the best available model at the moment. The problem of selecting a suitable boundary condition can maybe be solved by an experimental method presented in [6]. The extrapolation length can be determined by a measurement of the intensity angular correlation function of a speckle spot under a small rotation of the sample. The method can be applied for both transmission and diffuse reflection measurements.

The model used for evaluating the EBS measurements did not account for absorption of the light in the sample. This seem to have been a valid approximation since the absorption estimated by TOFS was very small in comparison to the scattering coefficient, namely 0.02 cm^{-1}. Further more, an non-neggligable absorption would have resulted in a roundening of the backscattering cone. However, the roundening of the cone that was observed seem to have been well accounted for by including the finite resoulition, in the form of the instrument respose function, into the calculation.

The fact that no significant roundening of the backscattering cone was observed also indicate that the approximation that the sample extended in a semi infinite space was valid. As mentioned earlier a significant transmission of light trough the sample would have demonstrated in a roundening of the cone. The validity of the approximation is also supported by a Monte Carlo simulation of

light propagation in a slab with approximately the same thickness and optical properties as the sample. The result from the simulation suggested that the optical transmission was below 2 %. The Monte Carlo simulation program that was used is descibed in [14].

The angular dependence of the incoherently scattered light was neglected in the experiment evaluation model, but could however be included. The bistatic coefficient for the incoherently scattered light (γ_l) can according to [5] be described by:

$$\gamma_l = 3\cos(\theta_s)\left(\tau_e + \frac{\cos(\theta_s)}{1+\cos(\theta_s)}\right)$$

In the detection angular range used in this set up, the model predicts a maximum variation of the baseline level of about 0.04 %. From considering the insecurity of the measurement it is clear that this variation could not be resolved and therfore do not need to be included in the explanatory model. If a much larger angular range needs to be covered or the internal reflection coefficient is assumed to be close to 1 it might, however, be a good idea to account for the angular dependence of the incoherently scattered light.

The enhancement factor acquired in the EBS experiment was significantly lower than the theoretical value of two, namely 1.6. An enhancement factor lower than two follows from a breaking of the time reverse symmetry. Practically this means that not all the light detected travels along a path were the light from a time reverse path could be simultaneously detected. There are two main reasons why this unwanted phenomena occurs.

Firstly, the light paths of the single scattered light lacks a time reversed counterpart. Hence, as explained before, a failure to effectively suppress the single scattered light will result in a lowering of the enhancement factor. There are strong reasons to believe that this was the case in this experiment. Replacing the sample with a mirror flips the helicity of all the incident light. Since the polarization optics on the detection side should let through only the helicity preserved light, there should in this case not be any detectable signal. However the images of the instrument response function were acquired with the polarization optics in place, so clearly there were still some light passing trough the polarization optics. The beam coming out on the detection side was very attenuated but could not be compleatly extinguished. Since the beam coulden't be sent straight into the camera non-attenuated, an investigation of the helicity filtering efficiency was never made. The somewhat poor performance of the polarization optics was probably due to low quality components.

Secondly, the enhancement factor is dependent on how large the detected field of view is in relation to the laser spot size. If the detected field of view is smaller the the laser spot, photons outside of the detection area are allowed to propagate into the field of view and be detected. Its time reverse will, however, not be detected, since it exits the sample outside of the field of view. This prevents detection of the time reverse symmetry. Correspondingly, if the detector field of view is larger than the illuminated spot size on the sample, the photons entering the sample inside the illuminated spot can exit outside and still be detected. These photon have no time reverse counterpart. To ensure a enhancement factor of two, the field of view of the detector should cover just the illuminated spot on the sample. For the set up discussed here, a field of

view smaller than the laser spot size yielded dark edges in the acquired images. The spot size was therefore set relatively small, probably at the cost of a smaller enhancement factor. The time symmetry breaking factors brought up here does not affect the shape of the EBS cone and should thus not introduce any systematical error into the measurements. However, an enhancement factor of two is desirable since it maximizes the signal to background ratio allowing an optimal utilization of the dynamic range of the detector. This in turn minimizes the statistical errors in the measurement.

This project have mainly focused on exploring and learning how to utilize EBS for measurements of scattering properties. A setup built for real application would of course need to be able to make measurements within a range of wavelengths, rather than just for one. Such a setup would need to include a spectrometer combined with a supercontinuum laser source [11] , alternatively a white light source [15].

Acknowledgements

We would like to thank everyone in the Biophotonics group at the Atomic Physics Division for the positive work environment. We would also like to direct a special thanks to Pontus Svenmarker for his help in the lab, Muhammad Saleem for interesting discussions and his ideas concerning the practical aspects of our setup and Arman Ahamed Subash for handling the TOFS measurements.

Above all, Stefan Andersson-Engels and Erik Alerstam, our supervisors, deserves a special recognition for providing us with an interesting project and for their ideas and encouragement.

Bibliography

[1] Thomas Svensson. *Pharmaceutical and biomedical applications of spectroscopy in the photon migration regime.* PhD thesis, Department of Physics, Lund University, 2008.

[2] Tomas Svensson, Erik Alerstam, Jonas Johansson, and Stefan Andersson-Engels. Optical porosimetry and investigations of the porosity experienced by light interacting with porous media. *Opt. Lett.*, 35:1740–1742, 2010.

[3] Tomas Svensson, Mats Andersson, Lars Rippe, Jonas Johansson, Staffan Folestad, and Stefan Andersson-Engels. High sensitivity gas spectroscopy of porous, highly scattering solids. *Opt. Lett.*, 33:80–82, 2008.

[4] H. C. Van De Hulst. *Light Scattering By Small Particles.* John Wiley & Sons, INC. , New York, USA, 1957.

[5] Boris Bret. *Multiple light scattering in porus gallium phosphide.* PhD thesis, Dept. Science and Technology, University of Twente, 2005.

[6] J.X Zhu, D.J Pine, and D.A Weitz. Internal reflection of diffusive light in random media. *Physical Review A*, 44:3948–3959, 1991.

[7] R. Corey, M. Kissner, and P. Saulnier. Coherent backscattering of light. *http://citeseerx.ist.psu.edu/viewdoc/summary?doi=10.1.1.123.8210.*

[8] Vladimir M. Turzhitsky, Jeremy D. Rogers, Nikhil N. Mutyal, Hemant K. Roy, and Vadim Backman. Characterization of light transport in scattering media at subdiffusion length scales with low-coherence enhanced backscattering. *IEEE Journal Of Selected Topics in Quantum Electronics*, Vol. 16:619–626, 2010.

[9] P.E. Wolf, G. Maret, E. Akkermans, and R. Maynard. Optical coherent backscattering by random media: an experimental study. *J. Phys. France*, 49:63–75, 1988.

[10] John Sawicki, Nikolaus Kastor, and Min Xu. Electric field monte carlo simulation of coherent backscattering of polarized light by a turbid medium containing mie scatterers. *Optics Express*, Vol. 16:5728–5738, 2008.

[11] O.L. Muskens and A. Lagendijk. Broadband enhanced backscattering spectroscopy of strongly scattering media. *Optics Express*, Vol. 16:1222–1231, 2008.

[12] D.S Wiersma and Meint P. van Albada. An accurate technique to record the angular distribution of backscattered light. *Review of Scientific Instruments*, Vol. 66:5473–5476, 1995.

[13] P. Gross, M. Störzer, S. Fiebig, M. Clausen, G. Maret, and C.M. Aegerter. A precise method to determine the angular distribution of backscattered light to high angles. *Review of Scientific Instruments*, 78:033105–033105–6, 2007.

[14] S. A. Prahl, M. Keijzer, S. L. Jacques, and A. J. Welch. A monte carlo model of light propagation in tissue. *SPIE Institute Series*, 5:102–111, 1989.

[15] Young L. Kim, Yang Liu, Vladimir M. Turzhitsky, Hemant K. Roy, Ramesh K. Wali, , and Vadim Backman. Coherent backscattering spectroscopy. *Opt. Lett.*, 29:1906–1908, 2004.

[16] Peter Niels den Outer. *Multiple light scattering in discrete random media; Coherent backscattering and imaging.* PhD thesis, University of Amsterdam, 1995.

[17] Ad Lagendijk, Rob Vreeker, and Pedro De Vries. Influence of internal reflection on diffusive transport in strongly scattering media. *Physics Letters A*, 136(1-2):81 – 88, 1989.

Appendix A

Theory of light transport in random materials

A.1 Photon migration

Considering light transport in a scattering material as a photon migration process, quite easily leads to the radiative transfer equation as a model for light transport . This is a balance equation of the photon density, $N(\vec{r}, \hat{s}, t)$ as a function of spatial coordinates $\vec{r}$, direction of flow $\hat{s}$ and time t. The scattering is introduced through a loss term. The photon density that is lost in one direction of flow to be scattered in to another direction is proportional to $c\mu_s$. Accounting for losses through absorption and scattering and adding a source term q yields radiative transfer equation for an arbitrary volume:

$$\frac{\partial N}{\partial t} = -c\nabla N \cdot \hat{s} - c(\mu_a + \mu_s)N + c\mu_s \int_{4\pi} p(\hat{s}', \hat{s})N(\hat{s}')d\omega'$$

Where $p(\hat{s}', \hat{s})$ is the so called phase function, which is a probability distribution of the scattering angle. To get the average intensity distribution the equation has to be integrated over all directions, which prevents an analytical solution. The way past this problem is usually to expand the photon density function in a isotropic part and one gradient part, neglecting higher order expansion terms. This is known as the diffusion approximation because it yields an equation that describes the light propagation as a diffusion process. This equation reads:

$$\frac{\partial \Phi(\vec{r}, t)}{\partial t} - D\nabla^2\Phi(\vec{r}, t) + c\mu_a\Phi(\vec{r}, t) = S(\vec{r}, t)$$

Where $\Phi(\vec{r}, t)$ is the fluence rate, which can be described as the amount of power incident on a infinitely small sphere at the position $\vec{r}$ normalized by its cross section area. $S(\vec{r}, t)$ is a source term and D is the diffusion coefficient which reads:

$$D = \frac{c}{3\mu_s'}$$

A detailed derivation following this path to the diffusion equation can be found in [1].

A.2 Wave propagation

The theoretical description made in this section follows the derivations made in [5], which is also much more exhaustive.

When considering light transport in turbid media as wave propagation in an ensemble averaged set of scatterers some simplifications of the conditions has to be made. As mentioned earlier only scalar waves can be modeled. The wave equation archived by transforming Maxwell's equation to the scalar case and disregarding the timedependence is known as Helmholtz equation. Another simplification made is that the transport media is modeled as point scatterers in a homogeneous material. The more physically correct approach to use the appropriate results from single scattering theory is mathematically difficult. The scatterers are thus modeled as delta functions. The effect of a single scattering event on a arbitrary wave function is given by the equation:

$$(\nabla^2 + k_0)\Psi(\mathbf{r}) = \int V(\mathbf{r}, \mathbf{r}')\Psi(\mathbf{r}')\mathbf{dr}'$$

Where $\Psi(\mathbf{r})$ is the wave function k_0 is the wavenumber of the incoming wave and $V(\mathbf{r}, \mathbf{r}')$ is the scattering potential, which in the case of a point scatterer can be written:

$$V(\mathbf{r}, \mathbf{r}') = V(\omega)\delta(\mathbf{r} - \mathbf{R})\delta(\mathbf{r}' - \mathbf{R}),$$

where $V(\omega)$ is the strength of the scattering potential, dependent on the frequency of the interacting light and $\mathbf{R}$ is the position of the scatterer. Formally this equation can be solved like:

$$\Psi(\mathbf{r}) = \Psi_{in}(\mathbf{r}) + \int g_0(\mathbf{r}, \mathbf{r_1})V(\mathbf{r_1}, \mathbf{r_2})\Psi(\mathbf{r_2})\mathbf{dr_1}\mathbf{dr_2}$$

This is known as the Lippman-Schwinger equation. Here $\Psi_{in}(\mathbf{r})$ is the wave function of the incoming wave and $g_0(\mathbf{r})$ is the free space Green function, i.e. the solution to the equation:

$$(\nabla^2 + k_0)g_0(\mathbf{r}', \mathbf{r}) = \delta(\mathbf{r}' - \mathbf{r})$$

Yielding the well known solution of a spherical wave traveling out from the position of the delta function.

$$g_0(r) = \frac{e^{ik_0 r}}{4\pi r}$$

The Green function of the scattering problem is given by an analog to the Lippman-Schwinger equation known as the Dyson-Schwinger equation.

$$g(\mathbf{r}, \mathbf{r}') = g(\mathbf{r} - \mathbf{r}') + \int g_0(\mathbf{r} - \mathbf{r}_1)V(\mathbf{r_1}, \mathbf{r_2})g(\mathbf{r_2}, \mathbf{r})d\mathbf{r_1}d\mathbf{r_2}$$

The Dyson-Schwinger equation can be recursively expanded by iteratively inserting the RHS into the place of the full Green function under the integral sign. Similarly, the Lippman-Schwinger can be solved by iteratively inserting the RHS into the place of the full wave function under the integral sign. Each order

of expansion can be considered as taking into account the effect of the scattering potential on the wave resulting from the previous order of expansion. Infinite expansion yields a new operator called the T-matrix, which fully describe the transformation of the incoming wave under scattering. The T-matrix is defined as:

$$T(\mathbf{r},\mathbf{r}') \equiv V(\mathbf{r},\mathbf{r}') + \int V(\mathbf{r}',\mathbf{r_1}) g_0(\mathbf{r_1},\mathbf{r_2}) V(\mathbf{r_2},\mathbf{r}) d\mathbf{r_1} d\mathbf{r_2} +$$
$$\int V(\mathbf{r}',\mathbf{r_1}) g_0(\mathbf{r_1},\mathbf{r_2}) V(\mathbf{r_2},\mathbf{r_3}) g_0(\mathbf{r_3},\mathbf{r_4}) V(\mathbf{r_4},\mathbf{r}) d\mathbf{r_1} d\mathbf{r_2} d\mathbf{r_3} d\mathbf{r_4} + \ldots$$

These types of expansions can be written in diagrams, where the integration is made implicit, in order to be more transperant. Let a ring represent the scattering potential, horizontal lines the free space Green function and a x the T-matrix, the above equation is then in diagram form written as:

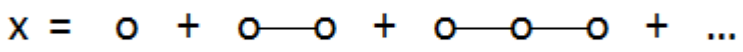

Figure A.1: Diagram of the T-matrix

If the T-matrix is known, the solution to the Lippman-Schwinger equation can be found as:

$$\Psi(\mathbf{r}) = \Psi_{in}(\mathbf{r}) + \int g_0(\mathbf{r},\mathbf{r_1}) T(\mathbf{r_1},\mathbf{r_2}) \Psi_{in}(\mathbf{r_2}) \mathbf{dr_1 dr_2}$$

And equivalently the Dyson-Swinger equation solves like:

$$g(\mathbf{r},\mathbf{r}') = \int g_0(\mathbf{r}',\mathbf{r_1}) T(\mathbf{r_1},\mathbf{r_2}) g_0(\mathbf{r_2},\mathbf{r}) d\mathbf{r_1} d\mathbf{r_2}$$

In the case of point scatterers the T-matrix is found to be proportional to the two delta functions found in the expression of the scattering potential. This makes the point scatterers easy to deal with when moving on to multiple scattering. A general result in scattering theory, which relates the T-matrix in Fourier space to the scattering crossection is the so called optical theorem:

$$\sigma_{ex} = \frac{ImT(k,k,\omega)}{k} = \int \frac{|T(k,k',\omega)|^2}{(4\pi)^2} d\widehat{k'} = \sigma_{sc}$$

This is only true for scattering of non absorbing particles. σ_{ex} is the extinction cross section which is a measure of how much light leaves its original propagation direction in the scattering process. In the case of absorption, the extinction cross section is the sum of the scattering and absorption cross sections.

Knowing how a single particle transforms an incoming wave, it is possible to derive how a wave is affected by multiple scattering. The relevant operator in the multiple scattering problem is known as the self energy operator and

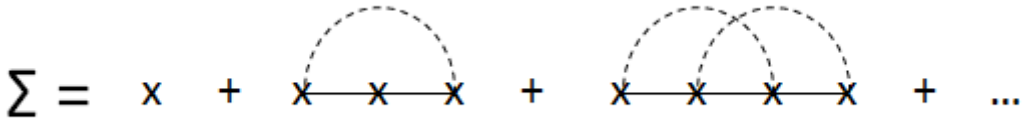

Figure A.2: Diagram of the self-energy operator

is denoted Σ. The name comes from its use within quantum mechanics. The self-energy operator in its diagram form is displayed in figure A.2:

The x represents as before the T-matrices and the horizontal lines free space Green functions. The dashed lines connect T-matrices for identical particles. E.g. the second term accounts for the influence it has on the total scattering process that wave is scattered once via another scatterer back to the same scatterer. There can be no dashed lines in-between two successive T-matrices, since recurrent scattering in one scatterer already is accounted for in the T-matrix itself. The self-energy operator contains all irreducible possible diagrams of the type stated above. An irreducible diagram is a diagram that cannot be broken down to lower order parts without breaking the dashed lines. The self energy operator is to the multiple scattering problem what the single particle scattering potential is in the single scattering case. The multiple scattering Dyson-Schwinger equation for the electrical field is:

$$g(\mathbf{r}, \mathbf{r}') = g(\mathbf{r} - \mathbf{r}') + \int g_0(\mathbf{r} - \mathbf{r}')\Sigma(\mathbf{r_1}, \mathbf{r_2})g(\mathbf{r_2}, \mathbf{r})d\mathbf{r_1}d\mathbf{r_2}$$

What is sought is the average field in an infinite space of scatterers. The averaging is taken care of by just considering Green functions and operators with a spatial dependence of the kind $r - r'$. This makes the problem translational invariant. Another way of looking at it, is to say that the material has the same properties independent of position.

Since there is no way of reducing the self energy operator to a closed expression, all but the first order term is neglected. This is called the independent scattering approximation since it neglects the effect subsequent scattering events have on the each scattering event. For this approximation to be valid, the density of scatterers has to be sufficiently low so that every scattering event actually can be considered as independent. I.e. scatterers should see each other in the far field. Under this approximation the wave can be considered as propagating as a free wave in between the scattering events. The averaged self energy operator in the independent scattering approximation is in Fourier space simply $\rho T(k, k)$, where ρ is the density of scatterers. The simplifications of the problem make it impossible to track the scattered wave. Only the non-scattered wave, also called the coherent wave, can be tracked.

Thanks to the averaging and the simplified operator, the Dyson-Schwinger equation is easily solved in Fourier space. The result is, as in the case with the free space Green function, a spherical wave but with a renormalized wave vector.

$$g(\mathbf{r}) = \frac{e^{iKr}}{4\pi r} = \frac{e^{-Im(K)}e^{iRe(K)r}}{4\pi r}$$

$$K = n\frac{\omega}{c} + i\frac{\mu_s}{2}$$

The imaginary part of the wave vector leads to exponential attenuation of the non-scattered wave. This is due to the relation between the imaginary part of the T-matrix and the extinction cross section introduced in the optical theorem. The real part of the T-matrix changes the wave vector by a factor n, which can thus be seen as a effective refractive index. The intensity of the coherent wave hence decreases with propagation length in the same manner as stated in the Beer-Lambert law. To account for both scattering and absorption, the scattering and absorption coefficients has to be added together.

An equation for the propagation of intensity has to be explicitly formulated, in order for the intensity of the scattered wave to be found. The intensity Green function or the intensity propagator is defined as:

$$G(r_1, r_2, r_3, r_4) \equiv g(r_1, r_2) \times g(r_3, r_4)$$

The relevant equation is the so called Bethe-Salpeter equation which is very much like a Dyson-Schwinger equation, but since it is an intensity equation, it contains both the field Green function and its complex conjugate.

$$G(r_1, r_2, r_3, r_4) = g(r_1, r_2)g(r_3, r_4)^* + \int g(r_1, r_a)g(r_3, r_c)^* U(r_a, r_b, r_c, r_d)G(r_b, r_3, r_d, r_4)dr_a dr_b dr_c dr_d$$

Where g is the electrical field Green function in the bulk material. The operator U contain all irreducible intensity propagation diagrams which is illustrated in figure A.3.

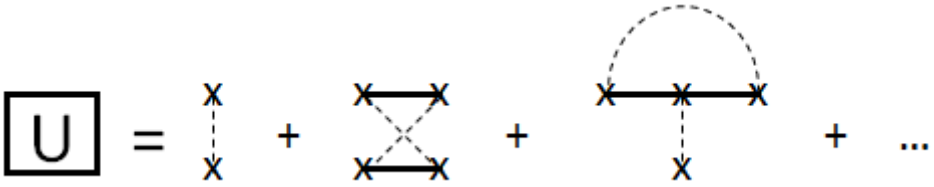

Figure A.3: Diagram of the U-operator

The lower part of the diagram represents the complex conjugated space and the thick horizontal lines the electrical field Green function in the bulk material. The Bethe-Salpeter equation cannot be solved analytically without further approximations. The simplest approximation that can be made is to just consider the first order diagram in U. Since this approximation only considers one scattering event at the time, the approach leads to a model where the intensity propagates from scatterer to scatterer. Hence, the model does not account for any interference effects. Just like the scattering potential, the U operator can be expanded. This expanded operator is denoted R. The part of

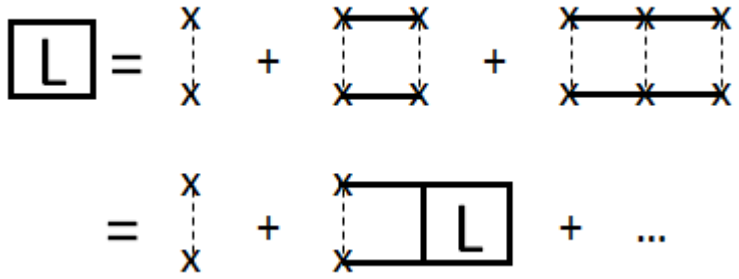

Figure A.4: Diagram of the L-operator

R that derives from the lowest order term in U is called L. Figure A.4 shows the first terms of the L-diagram, which for obvious reasons is called a ladder diagram.

As is apparent in the figure, the result of the expansion is an integral equation for L. Note that the last term in the diagram, excluding the two T-matrices, is the intensity propagator without the outgoing Green function within this approximation. I.e. the total operator in front of the incoming field under the integral sign in the solution to the Lippmann-Swinger equation. Thus multiplying both sides with the electrical field Green function and its complex conjugate yield an equation for the intensity propagator. Fourier transformed into momentum space, this equation can be showed to be equivalent with the radiative transfer equation. As mentioned before this equation can not be analytically solved, but from approximative assumptions it gives that the intensity propagation is governed by the diffusion equation. The stationary solution to this equation in an infinite medium with no absorption is:

$$G_d(r) = \frac{1}{4\pi r}$$

Hence this solution is not dependent on the reduced scattering coefficient as might be expected. However when looking at geometrys demanding boundary conditions like a semi infinite geometry or a slab geometry the reduced scattering coefficient becomes important.

A.3 Enhanced backscattering

The diagram expansion method presented in this chapter also allows for a derivation of the EBS curve shape, within the diffusion approximation. The equation for the L operator can be written in spatial coordinates as:

$$L(r_1, r_2, r_3, r_4) = \rho \left|t(\omega)\right|^2 \delta(r_1 - r_2)\delta(r_1 - r_3)\delta(r_1 - r_4) + F(r_1, r_2)\delta(r_1 - r_3)\delta(r_2 - r_4),$$

where $|t(\omega)|$ is the absolute value of the T-matrix and $F(r_1, r_2)$ is the intensity Green function. This factorization is only possible if the T-matrix is taken as proportional to a delta function. Let us return to the R operator. There is another contribution to this operator beyond the ladder terms that can be

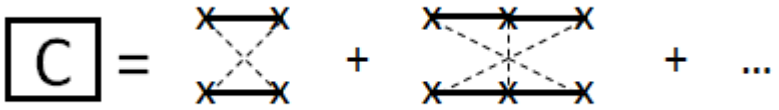

Figure A.5: Most crossed diagrams

considered and give a closed form expression. These are called the most crossed diagrams. These diagrams are illustrated in figure A.5

As might be clear from the appearance this diagram represents the effect from photons traveling along time-reversed paths. The complex conjugate part of the diagram visit all the same scatterers as the upper part but in the opposite order. Also notice the similarity with the ladder diagrams. In fact there is a simple trick involving the ladder diagrams which makes it easy to find a closed expression for the C operator. If the first order term in the L-diagram is dropped and the lower part is twisted 180° the diagrams look identical. Mathematically the twisting is done by switching place on the incoming and outgoing coordinates of the complex conjugate part of the equation. The C operator can thus in closed form in spatial coordinates be written:

$$C(r_1, r_2, r_3, r_4) = F(r_1, r_2)\delta(r_1 - r_4)\delta(r_2 - r_3)$$

There are two more functions that need to be known in order to get the backscattered intensity , namely the incoming field, ψ_{in} and the outgoing backscatter Green function, g_b. The incoming field is taken to be a plane wave attenuated by the scattering:

$$\psi(\mathbf{r}_1) = \sqrt{I_0} e^{iK_i \cdot \mathbf{r}_1}$$

Where the wave vector is:

$$\mathbf{K}_i = \mathbf{k_i} + i\frac{\widehat{\mathbf{z}}\mu_s}{2\cos(\theta_i)}$$

Where θ_i is the incoming angle of the light, $\mathbf{k_i}$, is the wave vector of the light outside the material and I_0 is the incoming intensity. This assumes that the boundary is located in the plane $z = 0$.

The backscattering outgoing Green function, corrected for the exit angle of the light, is taken to be [16]:

$$g_b(r_1, r_2) = -\frac{e^{ik_0 r_1}}{4\pi r_1} e^{i\mathbf{K_b}\cdot\mathbf{r_2}},$$

where $\mathbf{r_1}$ is far outside the bulk material and $\mathbf{r_2}$ is inside the bulk material, i.e. $\mathbf{r_2} << \mathbf{r_1}$. The backscattering wave vector is:

$$\mathbf{K_b} = \mathbf{k_s} + i\frac{\widehat{\mathbf{z}}\mu_s}{2\cos(\theta_s)},$$

where θ_s is the angle of backscattering and $\mathbf{k_s}$ is the wave vector of the wave scattered out of the medium.

Now since the problem is translational invariant in the x and y directions it is convenient to Fourier transform the intensity Green function along these coordinates. In that way the intensity Green function becomes a function of light penetration depth z and momentum transfer parallel to the boundary $q\perp$. It also has to be transformed so that it correctly include the mixed boundary conditions describes above. According to [17] the correct Green function to use is:

$$F(z_1, z_2, q_\perp) = G_d(z_1 - z_2, q_\perp) + \frac{z_e q_\perp - 1}{z_e q_\perp + 1} G_d(z_1 + z_2, q_\perp)$$

To arrive at a normalized way of describe angular resolved intensity the concept of bistatic coefficient has to be introduced. This is a way to express angular resolved intensity normalized to the incoming intensity, I_0, distance of observation, r, and the observed illuminated area $A\cos\theta_i$. The bistatic coefficient is denoted γ and is for a flat surface defined like:

$$\gamma \equiv \frac{4\pi r^2}{I_0 A \cos\theta_i}$$

Finally the curve shape of the EBS cone can be formulated in terms of a bistatic coefficient. The C operator, the incoming field and outgoing Green function are plugged in to the solution to the Lippmann-Schwinger problem. The first term of the solution containing just the incoming intensity is not included since this obviously will not contribute to the backscattered intensity. The solution integral is taken over the half infinite space z>0 and reads:

$$\gamma_c = \frac{1}{4\pi\cos\theta_i} \int\int F(z_1, z_2, q_\perp) \cos|u\mu_s'(z_1 - z_2)|\, e^{|v\mu_s'(z_1+z_2)|} dz_1 dz_2$$

Where γ_c is the bistatic coefficient for the coherent backscattering. The shorthands u and v are defined as:

$$u \equiv \frac{k_0}{\mu_s'} (\cos\theta_i - \cos\theta_s)$$

$$v \equiv \frac{1}{2} \left(\frac{1}{\cos\theta_s} + \frac{1}{\cos\theta_i} \right)$$

Integration yield the following expression for the bistatic coefficient of the coherently backscattered light.

$$\gamma_c = \frac{3}{2v\cos\theta_i} \frac{1}{(\alpha + v)^2 + u^2} \left(1 + \frac{2v\tau_e}{1 + \tau_e \alpha} \right)$$

Where the following shorthands have been introduced:

$$\alpha \equiv \frac{q_\perp}{\mu_s'}$$

$$\tau_e \equiv z_e \mu_s'$$

The momentum transfer parallel to the surface, $q_\perp$, is as before in the case of normal incidence $k_0 \sin\theta_s$.